JOURNAL OF GEOPHYSICAL RESEARCH, VOL. 108, NO. D24, 4784, doi:10.1029/2002JD002853, 2003

A global simulation of tropospheric ozone and related tracers: Description and evaluation of MOZART, version 2

Larry W. Horowitz,[1] Stacy Walters,[2] Denise L. Mauzerall,[3] Louisa K. Emmons,[2] Philip J. Rasch,[2] Claire Granier,[4,5] Xuexi Tie,[2] Jean-François Lamarque,[2] Martin G. Schultz,[6] Geoffrey S. Tyndall,[2] John J. Orlando,[2] and Guy P. Brasseur[6]

Received 16 August 2002; revised 10 May 2003; accepted 14 July 2003; published 24 December 2003.

[1] We have developed a global three-dimensional chemical transport model called Model of Ozone and Related Chemical Tracers (MOZART), version 2. This model, which will be made available to the community, is built on the framework of the National Center for Atmospheric Research (NCAR) Model of Atmospheric Transport and Chemistry (MATCH) and can easily be driven with various meteorological inputs and model resolutions. In this work, we describe the standard configuration of the model, in which the model is driven by meteorological inputs every 3 hours from the middle atmosphere version of the NCAR Community Climate Model (MACCM3) and uses a 20-min time step and a horizontal resolution of 2.8° latitude × 2.8° longitude with 34 vertical levels extending up to approximately 40 km. The model includes a detailed chemistry scheme for tropospheric ozone, nitrogen oxides, and hydrocarbon chemistry, with 63 chemical species. Tracer advection is performed using a flux-form semi-Lagrangian scheme with a pressure fixer. Subgrid-scale convective and boundary layer parameterizations are included in the model. Surface emissions include sources from fossil fuel combustion, biofuel and biomass burning, biogenic and soil emissions, and oceanic emissions. Parameterizations of dry and wet deposition are included. Stratospheric concentrations of several long-lived species (including ozone) are constrained by relaxation toward climatological values. The distribution of tropospheric ozone is well simulated in the model, including seasonality and horizontal and vertical gradients. However, the model tends to overestimate ozone near the tropopause at high northern latitudes. Concentrations of nitrogen oxides (NO_x) and nitric acid (HNO_3) agree well with observed values, but peroxyacetylnitrate (PAN) is overestimated by the model in the upper troposphere at several locations. Carbon monoxide (CO) is simulated well at most locations, but the seasonal cycle is underestimated at some sites in the Northern Hemisphere. We find that in situ photochemical production and loss dominate the tropospheric ozone budget, over input from the stratosphere and dry deposition. Approximately 75% of the tropospheric production and loss of ozone occurs within the tropics, with large net production in the tropical upper troposphere. Tropospheric production and loss of ozone are three to four times greater in the northern extratropics than the southern extratropics. The global sources of CO consist of photochemical production (55%) and direct emissions (45%). The tropics dominate the chemistry of CO, accounting for about 75% of the tropospheric production and loss. The global budgets of tropospheric ozone and CO are generally consistent with the range found in recent studies. The lifetime of methane (9.5 years) and methylchloroform (5.7 years) versus oxidation by tropospheric hydroxyl radical (OH), two useful measures of the global abundance of OH, agree well with recent estimates. Concentrations of nonmethane hydrocarbons and oxygenated intermediates (carbonyls and peroxides) generally agree

[1]Geophysical Fluid Dynamics Laboratory, NOAA, Princeton, New Jersey, USA.
[2]National Center for Atmospheric Research, Boulder, Colorado, USA.
[3]Woodrow Wilson School, Princeton University, Princeton, New Jersey, USA.
[4]Aeronomy Laboratory, NOAA, Boulder, Colorado, USA.
[5]Service d'Aeronomie, University of Paris, Paris, France.
[6]Max Planck Institute for Meteorology, Hamburg, Germany.

0148-0227/03/2002JD002853$09.00

well with observations. *INDEX TERMS:* 0322 Atmospheric Composition and Structure: Constituent sources and sinks; 0365 Atmospheric Composition and Structure: Troposphere—composition and chemistry; 0368 Atmospheric Composition and Structure: Troposphere—constituent transport and chemistry; 1610 Global Change: Atmosphere (0315, 0325); 3210 Mathematical Geophysics: Modeling; *KEYWORDS:* tropospheric ozone, chemical transport model, tropospheric chemistry

Citation: Horowitz, L. W., et al., A global simulation of tropospheric ozone and related tracers: Description and evaluation of MOZART, version 2, *J. Geophys. Res.*, *108*(D24), 4784, doi:10.1029/2002JD002853, 2003.

1. Introduction

[2] Ozone is of central importance in tropospheric chemistry. At high concentrations near the surface, it is harmful to humans and vegetation [*National Research Council*, 1991]. Photolysis of ozone, followed by reaction with water vapor, provides the primary source of the hydroxyl radical (OH), the primary atmospheric oxidant, in the troposphere [e.g., *Logan et al.*, 1981]. In addition, ozone is a significant greenhouse gas, particularly in the cold upper troposphere [*Hansen et al.*, 1997]. Photochemical production of tropospheric ozone is catalyzed by nitrogen oxides (NO_x = NO + NO_2) during the oxidation of CO and hydrocarbons.

[3] Several models of tropospheric ozone-NO_x-hydrocarbon chemistry have been developed and described recently [e.g., *Müller and Brasseur*, 1995; *Brasseur et al.*, 1998; *Hauglustaine et al.*, 1998; *Wang et al.*, 1998a, 1998b, 1998c; *Lawrence et al.*, 1999; *Levy et al.*, 1999; *Lelieveld and Dentener*, 2000; *Bey et al.*, 2001]. There are considerable differences among the models used in these studies, including in particular horizontal and vertical resolutions, emission inventories, chemical species and mechanism, meteorological fields, and method for calculating or specifying the stratosphere-troposphere exchange of ozone. The model we present in this work is highly flexible, has relatively fine horizontal and vertical resolution, and includes a fairly detailed representation of tropospheric ozone-NO_x-hydrocarbon chemistry with updated emission inventories. This model, which is designed to run efficiently on many types of computer architectures, will be made available to the community on the National Center for Atmospheric Research (NCAR) Atmospheric Chemistry Division (ACD) web site at http://acd.ucar.edu/models/MOZART/. A detailed description of the model is provided in section 2. Evaluation of model results is presented in section 3. The simulated global and regional budgets of tropospheric ozone and carbon monoxide are discussed in section 4. Discussion of the model results and conclusions are contained in section 5. A detailed listing of the chemical mechanism used in Model of Ozone and Related Chemical Tracers, version 2 (MOZART-2), is provided in the auxiliary material (Tables S1 and S2)[1].

2. Model Description

[4] MOZART-2 is a global chemical transport model designed to simulate the distribution of tropospheric ozone and its precursors. This model has been developed at multiple institutions, including the ACD of NCAR, the National Oceanic and Atmospheric Administration (NOAA) Geophysical Fluid Dynamics Laboratory (GFDL), the Max Planck Institute (MPI) for Meteorology, and Princeton University. This version of the model includes significant updates and improvements to the chemistry, emissions, and transport over version 1 of the model [*Brasseur et al.*, 1998]. MOZART-2 simulates the concentrations of 63 chemical species (Table 1) from the surface up to the lower stratosphere. The model can be driven with a variety of meteorological inputs, including data from a general circulation model, such as the NCAR Community Climate Model (CCM), or a meteorological reanalysis, such as those from the National Centers for Environmental Prediction (NCEP) and the European Centre for Medium-Range Weather Forecasts (ECMWF). In the configuration described in this paper, MOZART-2 is driven with meteorological inputs from the middle atmosphere version of the Community Climate Model (MACCM3) [*Kiehl et al.*, 1998]. In this version, the horizontal resolution is 2.8° latitude × 2.8° longitude with 34 hybrid vertical levels extending up to a pressure of 4 hPa (corresponding to an approximate altitude of 40 km), with a time step of 20 min for all chemistry and transport processes. The meteorological fields from MACCM3 improve the representation of stratosphere-troposphere exchange versus the tropospheric version of CCM-2 (Ω 0.5 library) used in MOZART-1. Versions of the model driven by other dynamical inputs, which have been used in analysis and forecasting for field campaigns including Tropospheric Ozone Production About the Spring Equinox (TOPSE) [*Emmons et al.*, 2003; *Tie et al.*, 2003] and Intercontinental Transport and Chemical Transformation of Anthropogenic Pollution Project 2002 (ITCT 2K2), will not be discussed in this paper.

[5] Meteorological parameters, including zonal and meridional winds, temperature, specific humidity, surface pressure, and surface fluxes of heat and momentum, are archived from an MACCM3 run and are provided to MOZART every 3 hours. MOZART is built on the framework of Model of Atmospheric Transport and Chemistry (MATCH) [*Rasch et al.*, 1997]. MATCH includes representations of advection, convective transport, boundary layer mixing, and wet and dry deposition. Convective mass fluxes are rediagnosed by MATCH, using the *Hack* [1994] scheme for shallow and midlevel convection and the *Zhang and McFarlane* [1995] scheme for deep convection, as in (MA)CCM-3. The addition of a deep convective scheme provides more realistic rapid transport of trace species from the surface to the upper troposphere than in MOZART-1, which included only the *Hack* [1994] scheme. Vertical diffusion within the boundary layer is represented using the parameterization of *Holtslag and Boville* [1993]. Ad-

[1] Auxiliary material is available via Web browser or via Anonymous FTP from ftp://agu.org/apend/jd/2002JD002853. Information on searching and submitting electronic supplements in found at http://www.agu.org/pubs/esupp_about.html.

Table 1. Chemical Species in MOZART

Species Name	Chemical Formula
O_x	$O_3 + O(^3P) + O(^1D)$
N_2O	N_2O
N	N
NO	NO
NO_2	NO_2
NO_3	NO_3
HNO_3	HNO_3
HO_2NO_2	HO_2NO_2
N_2O_5	N_2O_5
CH_4	CH_4
CH_3O_2	CH_3O_2
CH_3OOH	CH_3OOH
CH_2O	CH_2O
CO	CO
OH	OH
HO_2	HO_2
H_2O_2	H_2O_2
C_3H_6	C_3H_6
ISOP	C_5H_8
PO_2	$C_3H_6OHO_2$
CH_3CHO	CH_3CHO
POOH	C_3H_6OHOOH
CH_3CO_3	CH_3CO_3
CH_3COOOH	CH_3COOOH
PAN	$CH_3CO_3NO_2$
ONIT	$CH_3COCH_2ONO_2$
C_2H_6	C_2H_6
C_2H_4	C_2H_4
C_4H_{10}	C_4H_{10}
MPAN	$CH_2 = C(CH_3)CO_3NO_2$
$ISOPO_2$	$HOCH_2C(OO)(CH_3)CH = CH_2$
MVK	$CH_2 = CHC(O)CH_3$
MACR	$CH_2 = C(CH_3)CHO$
$MACRO_2$	$CH_3C(O)CH(OO)CH_2OH$
MACROOH	$CH_3C(O)CH(OOH)CH_2OH$
MCO_3	$CH_2 = C(CH_3)CO_3$
$C_2H_5O_2$	$C_2H_5O_2$
C_2H_5OOH	C_2H_5OOH
$C_{10}H_{16}$	$C_{10}H_{16}$
C_3H_8	C_3H_8
$C_3H_7O_2$	$C_3H_7O_2$
C_3H_7OOH	C_3H_7OOH
CH_3COCH_3	CH_3COCH_3
ROOH	CH_3COCH_2OOH
CH_3OH	CH_3OH
C_2H_5OH	C_2H_5OH
GLYALD	$HOCH_2CHO$
HYAC	CH_3COCH_2OH
EO_2	$HOCH_2CH_2O_2$
EO	$HOCH_2CH_2O$
HYDRALD	$HOCH_2C(CH_3) = CHCHO$
RO_2	$CH_3COCH_2O_2$
CH_3COCHO	CH_3COCHO
Rn-222	Rn-222
Pb-210	Pb-210
$ISOPNO_3$	$CH_2 = CHC(CH_3)(OO)CH_2ONO_2$
ONITR	$CH_2 = C(CH_3)CH(ONO_2)CH_2OH$
XO_2	$HOCH_2C(OO)(CH_3)CH(OH)CHO$
XOOH	$HOCH_2C(OOH)(CH_3)CH(OH)CHO$
ISOPOOH	$HOCH_2C(OOH)(CH_3)CH = CH_2$
H_2	H_2
stratospheric O_3	O_3 (stratospheric)
inert O_3	O_3 (stratospheric, inert)

vection of tracers is performed using the flux form semi Lagrangian advection scheme of *Lin and Rood* [1996] with a pressure fixer as described in section 2.4. The use of a flux form advection scheme is a major improvement over the semi Lagrangian scheme used in MOZART-1, in that it allows for tracer mass conservation and computes fluxes across grid cell boundaries, which can be used in computing species budgets (as in section 4). For computational efficiency, MOZART-2 uses only the lowest 34 vertical levels from MACCM3 (the full model has 52 levels extending up to 0.006 hPa). The additional MACCM3 layers in the upper stratosphere and mesosphere were found to be unnecessary for the simulation of tropospheric chemistry and transport (including stratosphere-troposphere exchange). Within the advection scheme, a rigid lid is imposed at the top of the MOZART-2 domain, and vertical velocities are rediagnosed based on the continuity equation. This artificial imposition of a rigid lid at 4 hPa causes only a minor error in the rediagnosed vertical velocities. This error is only significant in the upper stratosphere, where it does not affect our simulation because of the treatment of long-lived tracers in the stratosphere (see section 2.1). Vertical velocities near the tropopause and in the troposphere are nearly identical to those obtained by using all the 52 vertical levels. Chemical species are updated each time step by a sequence of operators: advection, surface emissions and dry deposition, vertical diffusion, convection, and wet deposition and chemistry.

[6] MOZART-2 is designed with a preprocessor that allows the model horizontal and vertical resolution, chemical species and reactions to be provided as input, and that generates the Fortran-90 source code based on these inputs. This allows considerable flexibility in specifying model resolution, chemical mechanism, emissions, output variables, and computer architecture. The chemical solver routines generated by the preprocessor are "hard-wired" to allow the evolution of the chemical species in the model to be solved more rapidly than using a general solver configured at runtime, while still affording the flexibility to easily change the chemical scheme.

2.1. Chemistry

[7] The chemical scheme used in MOZART-2 is considerably updated from that used in MOZART-1 [*Brasseur et al.*, 1998]. The chemical mechanism includes oxidation schemes for the nonmethane hydrocarbons (NMHCs): ethane, propane, ethene, propene, isoprene, α-pinene (as a surrogate for all terpenes), and *n*-butane (as a surrogate for all hydrocarbons with four or more carbons, excluding isoprene and terpenes). The 63 chemical species simulated by MOZART are listed in Table 1. Water vapor is prescribed based on the specific humidity field from MACCM3, which is read every 3 hours with other meteorological parameters. MACCM3 included a parameterization for the source of stratospheric water vapor from methane oxidation; photochemical production and loss of water vapor are not explicitly treated in MOZART-2. Kinetic reaction rates (auxiliary material, Table S1) have been updated from those used in MOZART-1, based on recent measurements, as compiled by *Sander et al.* [2000] and *Tyndall et al.* [2001]. The isoprene oxidation mechanism has been changed considerably from the simple scheme used in MOZART-1, based on the work by *Horowitz et al.* [1998], *Brocheton* [1999], and *Orlando et al.* [1999]. Heterogeneous reactions of N_2O_5 and NO_3 on sulfate aerosols are included in MOZART-2, using a prescribed sulfate aerosol distribution from a sulfate aerosol mass simulation performed in MOZART-1 [*Tie et al.*,

Table 2. Surface Emissions in MOZART

Species	Industry/Fossil Fuel	Biofuel Combustion	Biomass Burning	Biogenic/Soil	Oceans	Total
NO, Tg N yr^{-1}	23.11	1.25	9.81	6.62	0	40.79
CO, Tg yr^{-1}	306.89	231.04	486.63	160.10	10.00	1195.05
C_2H_6, Tg C y^{-1}	3.18	1.43	4.06	0.80	0.08	9.56
C_3H_8, Tg C yr^{-1}	5.02	0.47	1.10	1.64	0.11	8.33
C_2H_4, Tg C yr^{-1}	2.02	2.88	7.89	4.29	2.07	19.16
C_3H_6, Tg C yr^{-1}	0.86	1.42	2.81	0.86	2.52	8.46
C_4H_{10}, Tg C yr^{-1}	11.08	4.99	7.55	0	6.26	29.88
CH_3COCH_3, Tg yr^{-1}	1.00	0.11	2.51	19.95	13.45	37.02
ISOP, Tg C yr^{-1}	0	0	0	410.39	0	410.39
$C_{10}H_{16}$ Tg C yr^{-1}	0	0	0	129.06	0	129.06
CH_2O, Tg yr^{-1}	0.63	0.53	5.81	0	0	6.97
CH_3OH, Tg yr^{-1}	0	9.73	15.56	286.73	0	312.02
CH_4, Tg yr^{-1}[a]	94.97	14.01	71.84	145.69	9.98	489.47
N_2O, Tg yr^{-1}	5.00	0.16	1.72	20.73	11.31	38.92
H_2, Tg yr^{-1}	14.86	3.37	16.03	3.00	3.00	40.26

[a]The emissions for CH_4 also include 59.94 Tg yr^{-1} from rice cultivation and 93.05 Tg yr^{-1} from ruminants.

2001], with a reaction probability of $\gamma = 0.04$ [*Tie et al.*, 2003]. Photolysis frequencies (auxiliary material, Table S2) are computed using a precalculated multivariate interpolation table, derived from calculations conducted using the Tropospheric Ultraviolet and Visible radiation model ((TUV) version 3.0) [*Madronich and Flocke*, 1998], with the quantum yield of $O(^1D)$ from photolysis of ozone updated based on the work of *Sander et al.* [2000]. The lookup table gives clear-sky photolysis frequencies as a function of pressure, overhead ozone column, solar zenith angle, surface albedo, and temperature profile. Photolysis frequencies are adjusted for cloudiness by applying a cloud correction factor, as described by *Brasseur et al.* [1998]. The chemical system is solved numerically using a fully implicit Euler backward method with Newton-Raphson iteration.

[8] Stratospheric concentrations of several long-lived species (O_3, $NO_x = NO + NO_2$, HNO_3, N_2O_5, and N_2O) are constrained by relaxation toward zonally and monthly averaged values from the middle atmosphere model Study of Transport and Chemical Reactions in the Stratosphere (STARS) [*Brasseur et al.*, 1997] (for species other than O_3) and from ''observed'' ozone climatologies from *Logan* [1999] (for O_3 below 100 mb) and the Halogen Occultation Experiment (HALOE) [*Randel et al.*, 1998] (for O_3 above 100 mb). This relaxation is performed from the local thermal tropopause (defined by a lapse rate of 2 K km^{-1}) to the model top at each time step, with a relaxation time constant of 10 days. Concentrations of CH_4 and CO are also prescribed in the top two model levels (down to 6 hPa), based on model results from STARS.

2.2. Emissions

[9] Surface emissions of chemical species in MOZART include those from fossil fuel burning and other industrial activity, biomass burning, biogenic emissions from vegetation and soils, and oceanic emissions. The emissions in MOZART are intended to be representative of those in the early 1990s. The surface emissions used in the model are summarized in Table 2. Monthly mean emissions of NO_x from various source types, for January and July, are shown in Figure 1. Biomass burning sources include forest burning, savannah burning, and agricultural waste burning. Biofuel combustion includes fuelwood burning. Emissions from fossil fuel combustion, fuelwood burning, and agricultural waste burning are based on the Emission Database for Global Atmospheric Research (EDGAR) v2.0 inventory [*Olivier et al.*, 1996], with seasonality from the Intermediate Model for the Global and Annual Evolution of Species (IMAGES) [*Müller*, 1992]. For CO, emissions from agriculatural waste and fuelwood burning were modified from those in EDGAR v2.0 based on preliminary estimates from EDGAR v3.0 [*Olivier and Berdowski*, 2001], by scaling to give 16 and 231 Tg yr^{-1}, respectively. The spatial and temporal distribution of the amount of biomass burned is taken from *Hao and Liu* [1994] in the tropics and from *Müller* [1992] in the extratropics. Emission ratios of chemical species from biomass burning are based on the recent review by *Andreae and Merlet* [2001]. Biogenic emissions of hydrocarbons from vegetation are taken from Global Emissions Inventory Activity (GEIA) [*Guenther et al.*, 1995] for isoprene and monoterpenes, and from *Müller* [1992] for other species. The isoprene emissions in the tropics are reduced by 25% from the estimates of *Guenther et al.* [1995], based on more recent studies indicating that *Guenther et al.* [1995] may have overestimated isoprene emissions from tropical rain forests [e.g., *Klinger et al.*, 1998] (similar reductions in the tropics were included by *Bey et al.* [2001]). Biogenic emissions of methanol are included at an annual rate of 287 Tg yr^{-1} based approximately on the emission ratio to isoprene found by *Guenther et al.* [2000] for North America, with spatial distribution and seasonality specified based on that used for higher hydrocarbons by *Müller* [1992]. Emissions of NO_x from microbial production in soils are taken from *Yienger and Levy* [1995], with soil emissions of CO, N_2O, and H_2 from *Müller* [1992]. Biogenic emissions of methane from rice paddies and ruminants are based on EDGAR [*Olivier et al.*, 1996], while those from wetlands and termites are based on the work of *Müller* [1992]. Emissions of CO, methane, and NMHCs from the ocean are included in the model, with distributions as in the work of *Brasseur et al.* [1998] but with reduced magnitudes (reduction factor is approximately 10 for alkanes, 4 for alkenes, and 2 for CO), based on more recent estimates. Oceanic emissions of acetone are also included, with a magnitude of 13.5 Tg yr^{-1}, located

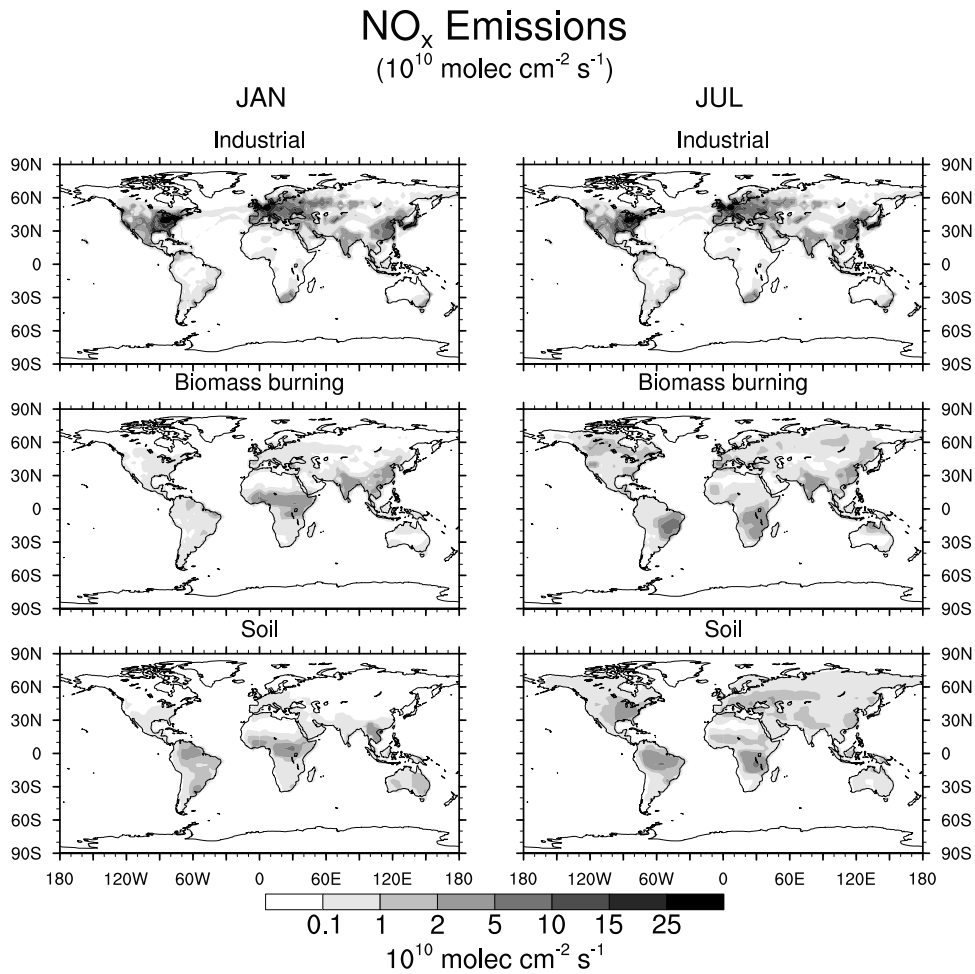

Figure 1. Monthly mean surface emissions (in units of 10^{10} molecules cm^{-2} s^{-1}) of nitrogen oxides (as NO) from industrial sources (top), biomass and biofuel burning (middle), and biogenic emissions from soil (bottom) for January (left) and July (right). See color version of this figure at back of this issue.

primarily in the tropics [e.g., *Jacob et al.*, 2002]. These emissions are available, at various horizontal resolutions, from the MOZART web site, http://acd.ucar.edu/models/MOZART/.

[10] Lightning is distributed in the model according to the location of convective clouds, as diagnosed by the MATCH scheme. The corresponding source of NO_x is parameterized following the work of *Price et al.* [1997], with a "C-shaped" vertical profile [*Pickering et al.*, 1998]. According to the *Price et al.* [1997] parameterization, the lightning frequency depends strongly on the convective cloud top height, and the ratio of cloud-to-cloud versus cloud-to-ground lightning depends on the cold cloud thickness (from 0°C to the cloud top). The lightning source is scaled to provide a total of 3.0 Tg N (as NO) per year, with significant diurnal and seasonal fluctuations based on the model meteorology. The value of 3.0 Tg N yr^{-1} used in this study is within the range of 3–5 Tg N yr^{-1} estimated by *Levy et al.* [1996] but is well below the range of 5–20 Tg N yr^{-1} estimated by *Price et al.* [1997]. Most recent global modeling studies have used NO_x sources from lightning in the range of 3–7 Tg N yr^{-1} [e.g., *Brasseur et al.*, 1998; *Levy et al.*, 1999; *Lelieveld and Dentener*, 2000; *Bey et al.*, 2001]. Aircraft emissions of NO_x and CO are included in the model, based on the work of *Friedl* [1997], with magnitudes of 0.67 Tg N yr^{-1} (NO) and 1.44 Tg yr^{-1} (CO).

2.3. Dry Deposition and Wet Scavenging

[11] Dry deposition velocities are included in the model for O_3, HNO_3, NO_2, CO, hydrogen peroxide (H_2O_2), organic hydroperoxides, carbonyl compounds, HO_2NO_2, peroxyacylnitrates (PANs) and other organic nitrates, alcohols, CH_4, NO, Pb-210, and H_2. The deposition velocities are calculated off-line using a resistance-in-series scheme [*Wesely*, 1989; *Hess et al.*, 2000] driven by 10 years of meteorological fields from NCEP reanalyses every 6 hours. The monthly mean of the calculated values are then computed and used in the model. The calculation of surface resistances uses the vegetation distribution of *DeFries and Townshend* [1994]. The calculation is done on a 1° × 1° grid and then averaged to the model resolution taking into account the different vegetation types within each grid cell. A diurnal cycle is imposed on the monthly mean deposition velocity for O_3 as in the work of *Brasseur et al.* [1998].

[12] Wet deposition is represented as a first-order loss process within the chemistry operator, with loss rates computed based on the large-scale and convective precip-

itation rates diagnosed by MATCH. Soluble species, HNO_3, H_2O_2, CH_2O, organic hydroperoxides (CH_3OOH, C_2H_5OOH, C_3H_7OOH, POOH, ROOH, ISOPOOH, MACROOH, and XOOH), CH_3COOOH, CH_3COCHO, HO_2NO_2, alkyl nitrates (ONIT, ONITR, $ISOPNO_3$), MVK, MACR, GLYALD, HYAC, CH_3CHO, alcohols (CH_3OH and C_2H_5OH), and Pb-210, undergo wet removal by in-cloud scavenging, using the parameterization of *Giorgi and Chameides* [1985] based on their temperature-dependent effective Henry's law constants. In addition, highly soluble species (HNO_3, H_2O_2, ONIT, ISOPOOH, MACROOH, XOOH, and Pb-210) are also removed by below-cloud washout, using the formulation described in detail by *Brasseur et al.* [1998]. The wet deposition scheme used here differs from that used in MOZART-1 in that in-cloud removal of highly soluble species is treated using the *Giorgi and Chameides* [1985] parameterization rather than the *Brasseur et al.* [1998] scheme as was done in MOZART-1. This change considerably increases the wet removal of these species and greatly improves agreement of HNO_3 concentrations and wet deposition fluxes with observations (see section 3.2).

2.4. Pressure Fixer

[13] Mass consistency problems with advection schemes in off-line tracer transport models in general, including the *Lin and Rood* [1996] scheme, lead to nonconservation of tracer mass. This effect results from the inconsistency between the vertically integrated mass convergence computed by the advection scheme and the surface pressure tendency interpolated from the dynamical input files. A more complete discussion of this issue is provided by *Jöckel et al.* [2001]. The pressure fixer developed by P. Cameron-Smith at Lawrence Livermore National Laboratory (LLNL) (P. Cameron-Smith, personal communication, 2002; http://asd.llnl.gov/pfix/) is used in MOZART-2 to modify the horizontal mass fluxes so as to achieve consistency with the surface pressure tendency archived from the MACCM, eliminating the problem of mass inconsistency and tracer nonconservation. The pressure fixer typically imposes only a small change on the horizontal wind fields and does not alter large-scale circulation features. If the pressure fixer were omitted in MOZART-2, running with MACCM3 meteorological inputs, this nonconservation would produce an anomalous source of ozone in the vicinity of the tropopause (where the vertical gradient of the ozone-mixing ratio is large) of approximately 187 Tg yr^{-1} (87 Tg yr^{-1} of this total is within the troposphere, as defined in the budget analysis in section 4).

3. Model Evaluation

[14] The model is driven by meteorology from the MACCM3 general circulation model. This meteorology is intended to simulate a "typical" year, not any specific year of observations. In order to compare model results with observations, a multiyear climatology throughout the troposphere would be desirable. Such a climatology is only available at a large number of sites for ozone, based on long-term ozonesonde measurements (e.g., those compiled by *Logan* [1999]). For ozone, we compare monthly (or seasonal) mean model results with the corresponding multiyear mean observations. For other species, such as CO, NO_x, PAN, HNO_3, acetone, H_2O_2, and NMHCs, we compare model results with observations obtained from aircraft campaigns, as compiled by *Emmons et al.* [2000]. For these species, we compare mean regional vertical profiles observed during a given field campaign with model results averaged over the same geographical region and time period. A detailed description of the method used to construct the observed regional mean profiles from the raw observations is given by *Emmons et al.* [2000]. For CO, we also compare model results with multiyear surface observations from the NOAA/Climate Monitoring and Diagnostics Laboratory (CMDL) flask measurement network [*Novelli et al.*, 1998]. Additional comparisons between MOZART-2 model results and observations are available on the MOZART web page located at http://acd.ucar.edu/models/MOZART/.

3.1. Ozone

3.1.1. Vertical Profiles

[15] The modeled monthly mean concentrations of ozone near the surface and at 500 hPa are shown (for January and July) in Figure 2. Ozone concentrations at northern midlatitudes increase dramatically from January to July near the surface (and to a lesser extent in the middle troposphere), as a result of photochemical production of ozone, which requires high concentrations of NO_x and other precursors, as well as ultraviolet radiation. In biomass burning regions of South America and southern Africa, an increase in near-surface ozone can also be seen from January to July, reflecting the seasonal cycle of biomass burning, which provides the precursors for ozone production. Ozone concentrations generally increase with height, outside the regions of strong ozone production near the surface. This results from subsidence of ozone-rich air from the upper troposphere and the stratosphere.

[16] Simulated vertical profiles of ozone are compared with ozonesonde observations in Figure 3. The observations are from multiple years of sonde measurements, as compiled by *Logan* [1999]. The simulated magnitude and vertical gradient of ozone are generally in good agreement with observations. At tropical and subtropical locations (e.g., Hilo, Brazzaville, Natal, and Samoa), the model simulates well the observed magnitude and vertical structure of ozone, including relative maxima in many of the profiles in the lower to middle troposphere above the boundary layer. At high northern latitudes, the model tends to overestimate ozone in the vicinity of the tropopause at several sites by 25% or more (e.g., Alert, Churchill), particularly in winter. The observations in the tropopause region at these stations tend to show large variability, probably indicating large variations in tropopause height. The agreement with observations is generally better at northern midlatitudes (Cape Kennedy and Hohenpeissenberg), although even at these sites the model tends to overestimate ozone near the tropopause in certain seasons. Larger discrepancies remain at several other midlatitude stations (e.g., Kagoshima). The model overestimate of ozone in the upper troposphere in the northern extratropics may result from inadequate resolution of the tropopause or

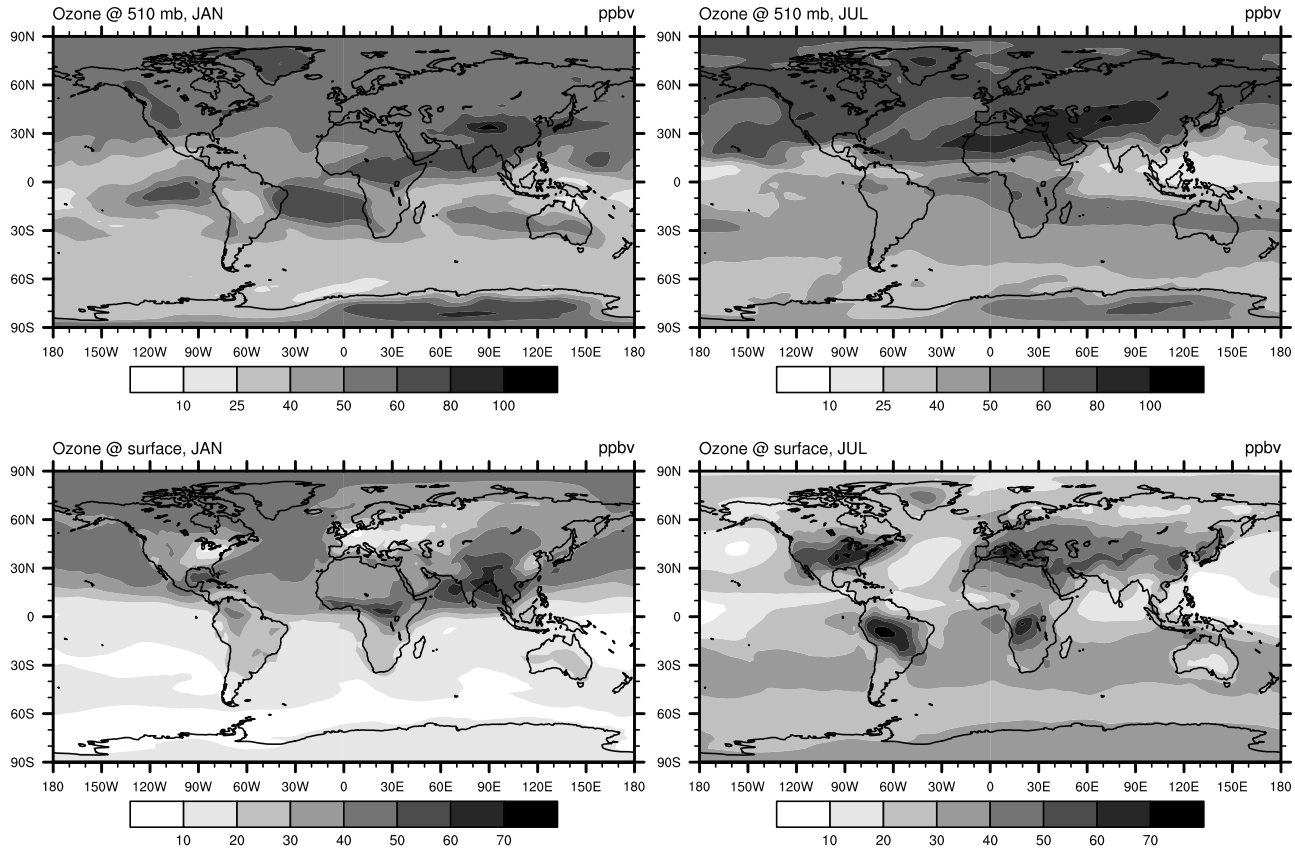

Figure 2. Monthly mean simulated concentrations of ozone (in ppbv) in January (left) and July (right) at hybrid model levels corresponding approximately to 970 (bottom) and 510 hPa (top). See color version of this figure at back of this issue.

excessive cross-tropopause transport of ozone by advection at these latitudes in the model, despite the relatively low global stratosphere-troposphere flux of ozone in the model (see section 4.1). Also, ozone production in the middle and upper troposphere in the northern extratropics (see section 4.1) may be excessive in the model, contributing to the overestimation of ozone in this region.

[17] Overall, the agreement between simulated and observed ozone is improved considerably from that obtained with MOZART-1 [*Hauglustaine et al.*, 1998], in which tropospheric ozone was systematically too low, particularly at high latitudes and high altitudes. This improvement results from a variety of improvements to the model, in particular the advection scheme, the dynamical inputs, stronger convective transport to the upper troposphere, and improved chemical scheme and emissions. The semi-Lagrangian advection scheme used in MOZART-1 was nonconservative and required a mass fixer, which had a large, but artificial, effect on ozone in the region of the tropopause, where vertical gradients are large. The convective transport in MOZART-1 was parameterized using the *Hack* [1994] scheme, which is used in MOZART-2 for shallow and midlevel convection only. This scheme differs from the *Zhang and McFarlane* [1995] scheme, used in MOZART-2 for deep convection, in that it lacks penetrative deep convective plumes. The *Hack* [1994] scheme may underestimate deep vertical mixing [*Brasseur et al.*, 1998], while the *Zhang and McFarlane* [1995] scheme is more effective at transporting ozone precursors from the surface to the upper troposphere, enhancing ozone production in the upper troposphere. This enhancement in upper tropospheric ozone production associated with stronger deep convection may be excessive with the *Zhang and McFarlane* [1995] scheme. Further evaluation of the strength of convective transport, and its impact on ozone, is necessary.

3.1.2. Seasonal Variation

[18] The seasonal variation of simulated ozone-mixing ratios at three pressure levels (800, 500, and 300 hPa) is compared with observations in Figure 4. At 800 hPa, the simulated seasonal cycle of ozone agrees well with observations at most sites. Northern midlatitude sites tend to show a seasonal maximum during spring to summer at this level (e.g., Hohenpeissenberg), reflecting the seasonal cycle of photochemical ozone production and possibly stratospheric influence. The model simulates this general feature of the observations but shifts the maximum several months too late at Wallops Island. In the southern tropics (e.g., Ascension Island), the observations indicate peak ozone concentrations during July–September (depending on location), reflecting the combined influences of biomass burning emissions and dynamics [*Moxim and Levy*, 2000]. The model tends to reproduce approximately the timing and the magnitude of this maximum.

[19] In the midtroposphere, at 500 hPa, the seasonal maximum of ozone at northern extratropical sites typically occurs in the late spring (May–June). The model reproduces

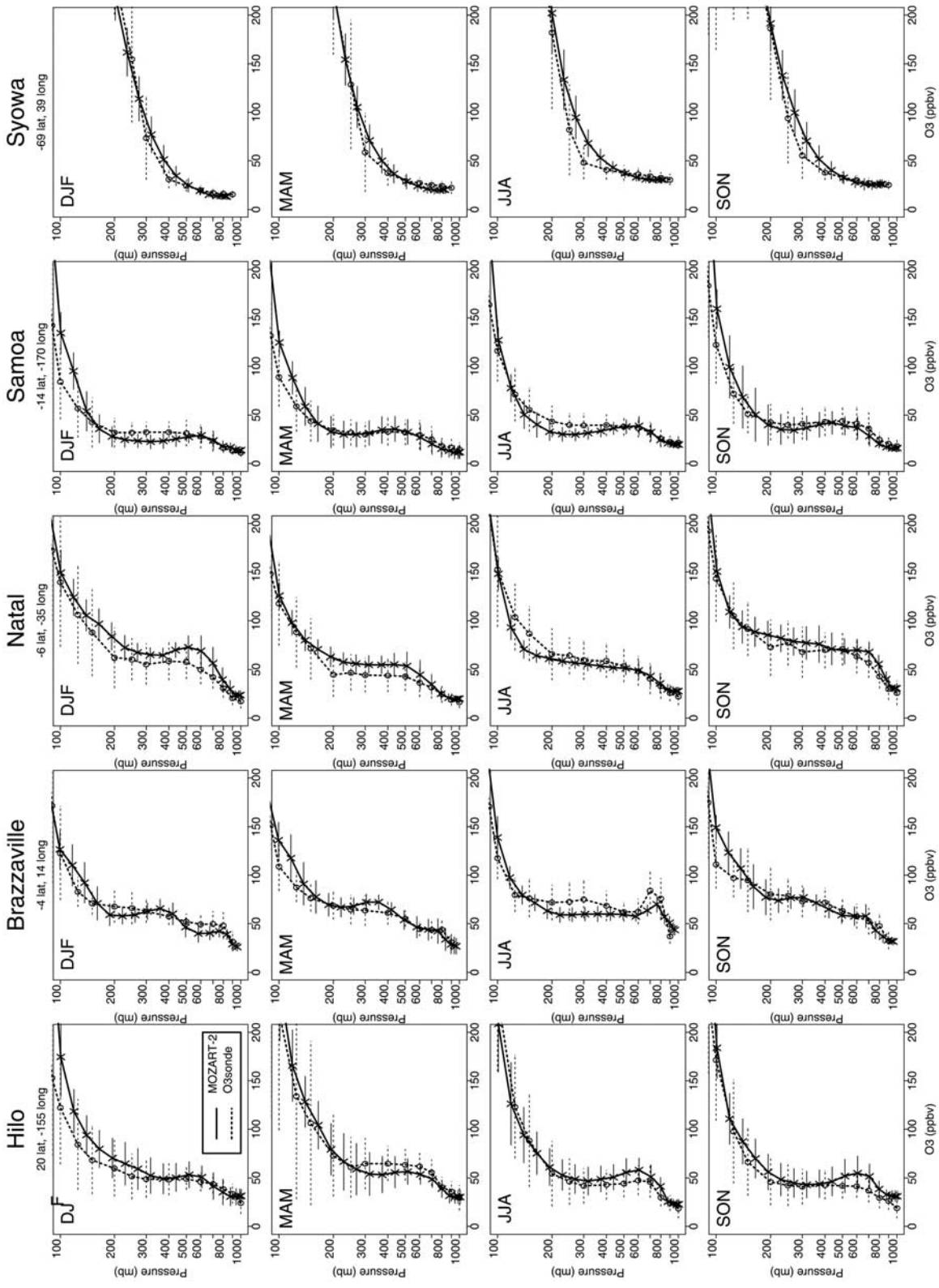

Figure 3. Comparison of observed (dotted lines) and simulated (solid lines) seasonal vertical profiles of ozone volume mixing ratio (ppbv), and standard deviations (horizontal lines). Observations are from ozonesonde measurements compiled by *Logan* [1999]. Station names and locations (latitude and longitude) are given above each plot. See color version of this figure in the HTML.

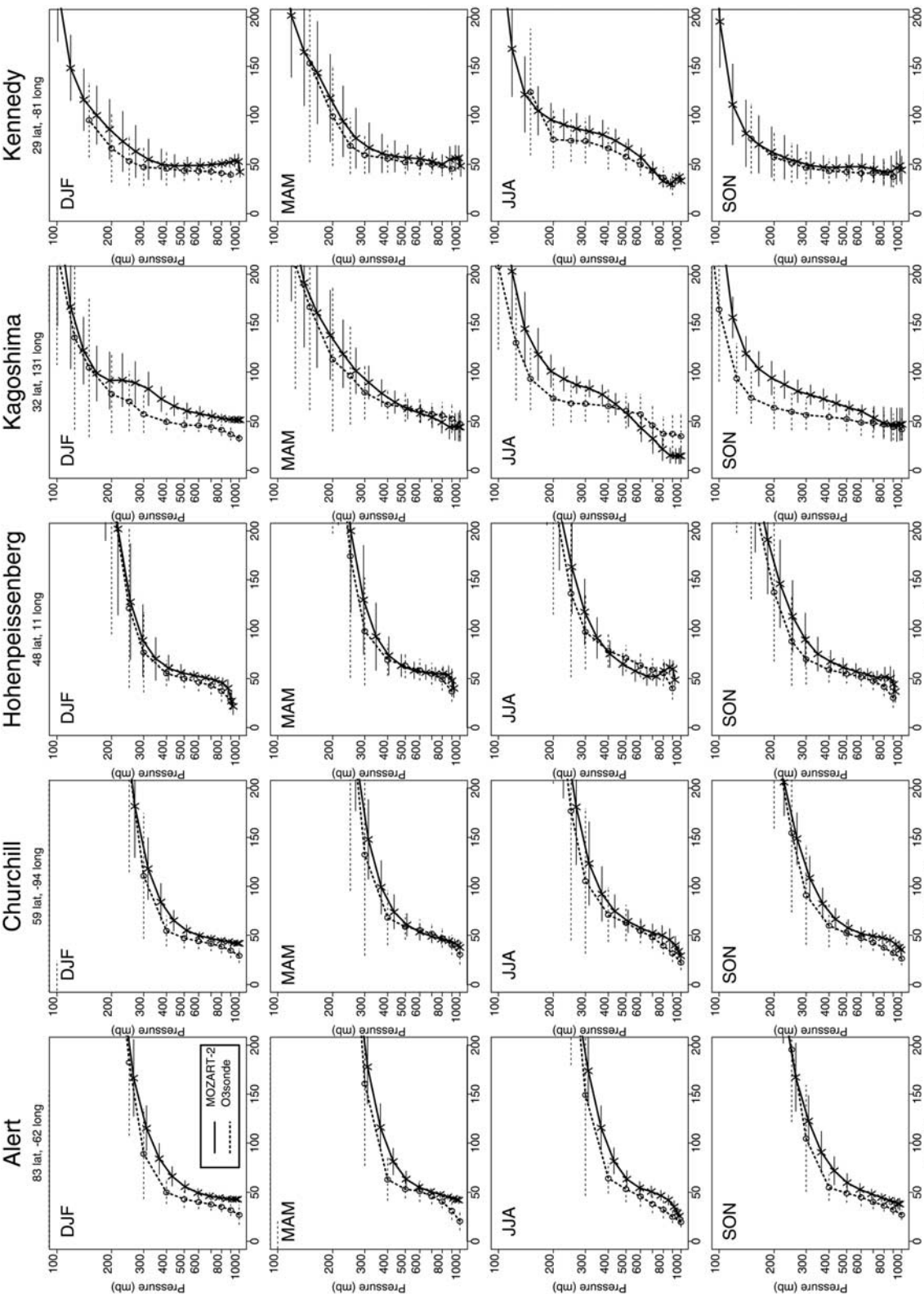

Figure 3. (continued)

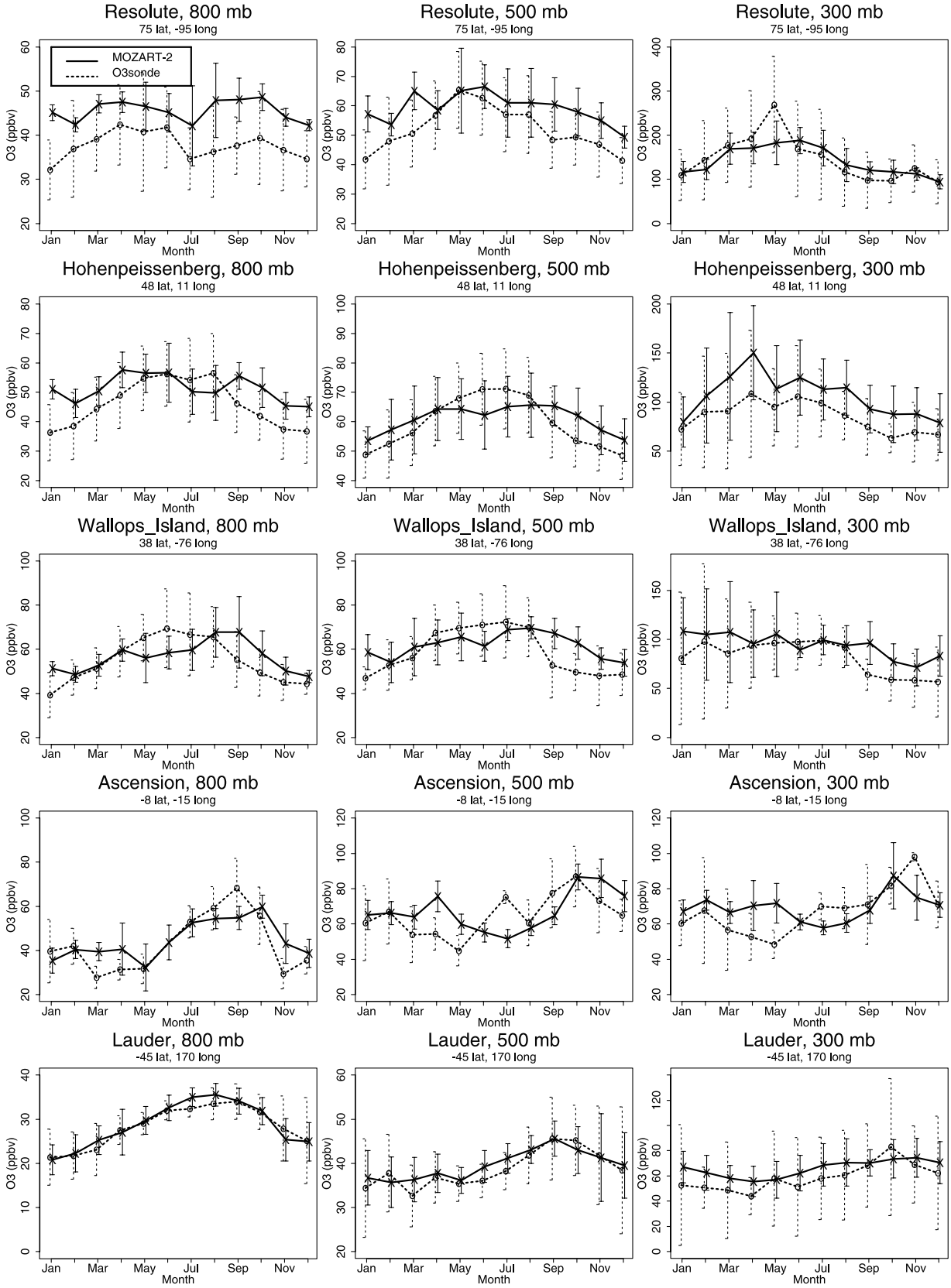

Figure 4. Monthly mean observed (dotted lines) and simulated (solid lines) ozone volume mixing ratios (ppbv), and standard deviations (vertical lines) at vertical levels of 800 (left), 500 (center), and 300 hPa (right). Station names and locations (latitude and longitude) are given above each plot. Observations are from ozonesonde measurements compiled by *Logan* [1999]. See color version of this figure in the HTML.

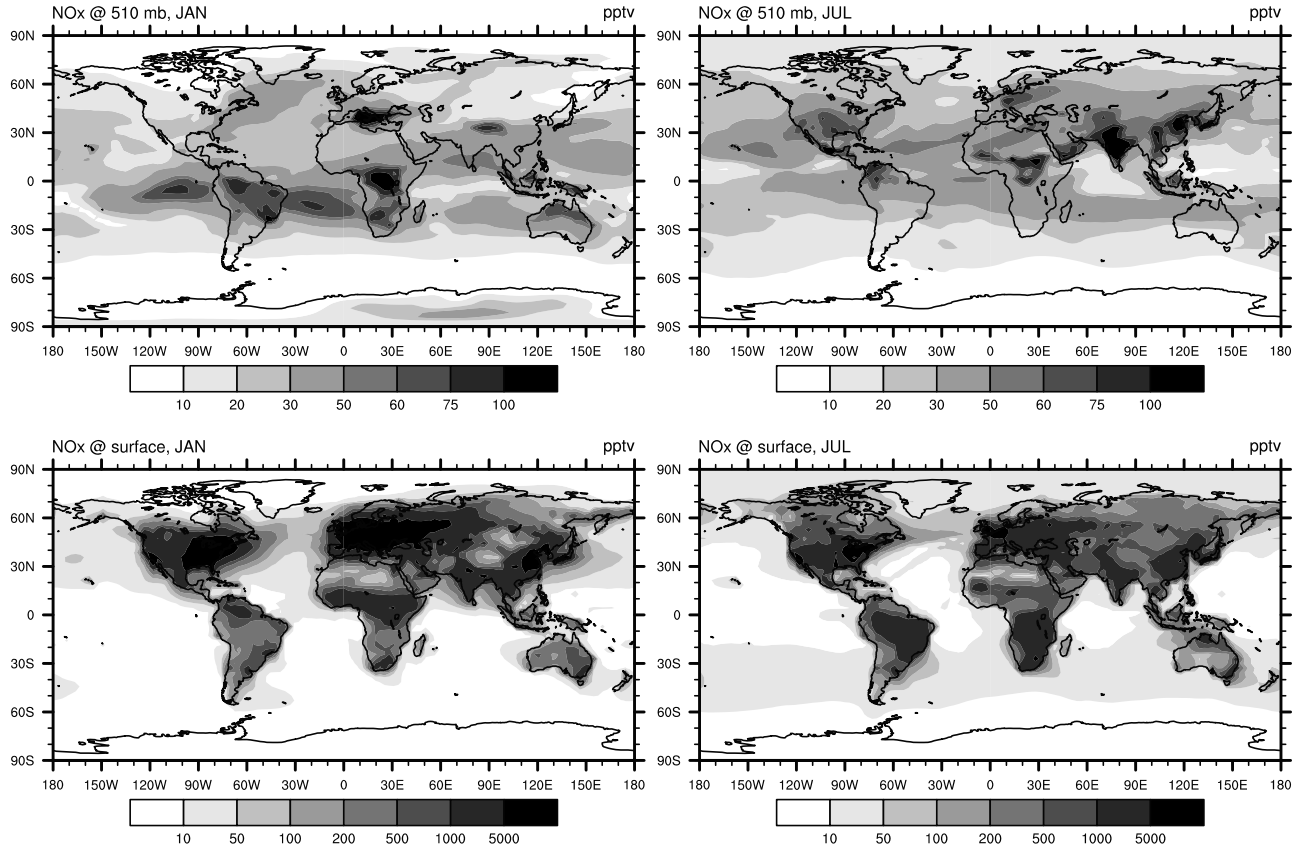

Figure 5. Same as Figure 2 but for NO_x ($NO + NO_2$) (in pptv). See color version of this figure at back of this issue.

this feature at most sites. However, ozone at Resolute is overestimated by about 20% throughout much of the year. This overestimate results in part from excessive downward transport from the upper troposphere at high northern latitudes in the model.

[20] In the upper troposphere, at 300 hPa, the model captures the observed seasonality of ozone at most sites. At high-latitude sites, the simulated ozone concentrations at this level are strongly influenced by the relaxation to the observed climatology that is performed in the stratosphere. As mentioned in the previous section, the model tends to overestimate ozone near the tropopause at some sites at northern middle to high latitudes, such as that at Hohenpeissenberg, where ozone is overestimated by ~25% in some months.

3.2. Nitrogen Species

[21] Simulated monthly mean concentrations of NO_x are shown in Figure 5. High NO_x concentrations are present near the surface over regions with strong emissions of NO_x from fossil fuel combustion (e.g., North America and Europe), biomass burning (South and East Asia, South America, and Africa), or other sources. The seasonal cycle of NO_x near the surface may be controlled by the seasonality of emissions (especially in the case of biomass burning), or by chemistry and transport (e.g., over North America, where chemical loss is slower during the winter, as is the ventilation of the continental boundary layer). Midtropospheric NO_x concentrations reflect transport from surface sources, as well as in situ production from lightning (see section 2.2). Comparisons of simulated and observed vertical profiles of NO_x, PAN, and HNO_3 are shown in Figures 6–8, respectively. The regions used for these profile comparisons are listed in Table 3.

[22] Predicted NO_x concentrations are generally in very good agreement with the observed values, given the large spatial and temporal variability in this short-lived species (Figure 6). The model overestimates values near the surface over some island locations, e.g., Japan_Coast_E in PEM-West-A/B and Hawaii in PEM-Tropics-B (not shown), because terrestrial emissions are spread throughout the entire model gridbox, while the measurements may sample the clean marine boundary layer. Good agreement with observations is seen in the upper troposphere at all locations except New Zealand (in PEM-Tropics-A, not shown), suggesting that the source of NO_x from lightning in MOZART is approximately correct.

[23] Concentrations of PAN in the model tend to increase strongly with altitude at most sites, with maximum mixing ratios appearing in the upper troposphere. This reflects the very long thermal decomposition time of PAN in the cold upper troposphere and the slow loss by photolysis (with a lifetime of about a month). PAN is either transported to the upper troposphere by rapid convection or is formed there by reactions of its precursors, hydrocarbons (which are transported to the upper troposphere by convection), and NO_x (which has a strong upper tropospheric source from lightning). These profiles agree with observations at many sites, although there are a significant number of regions at low to

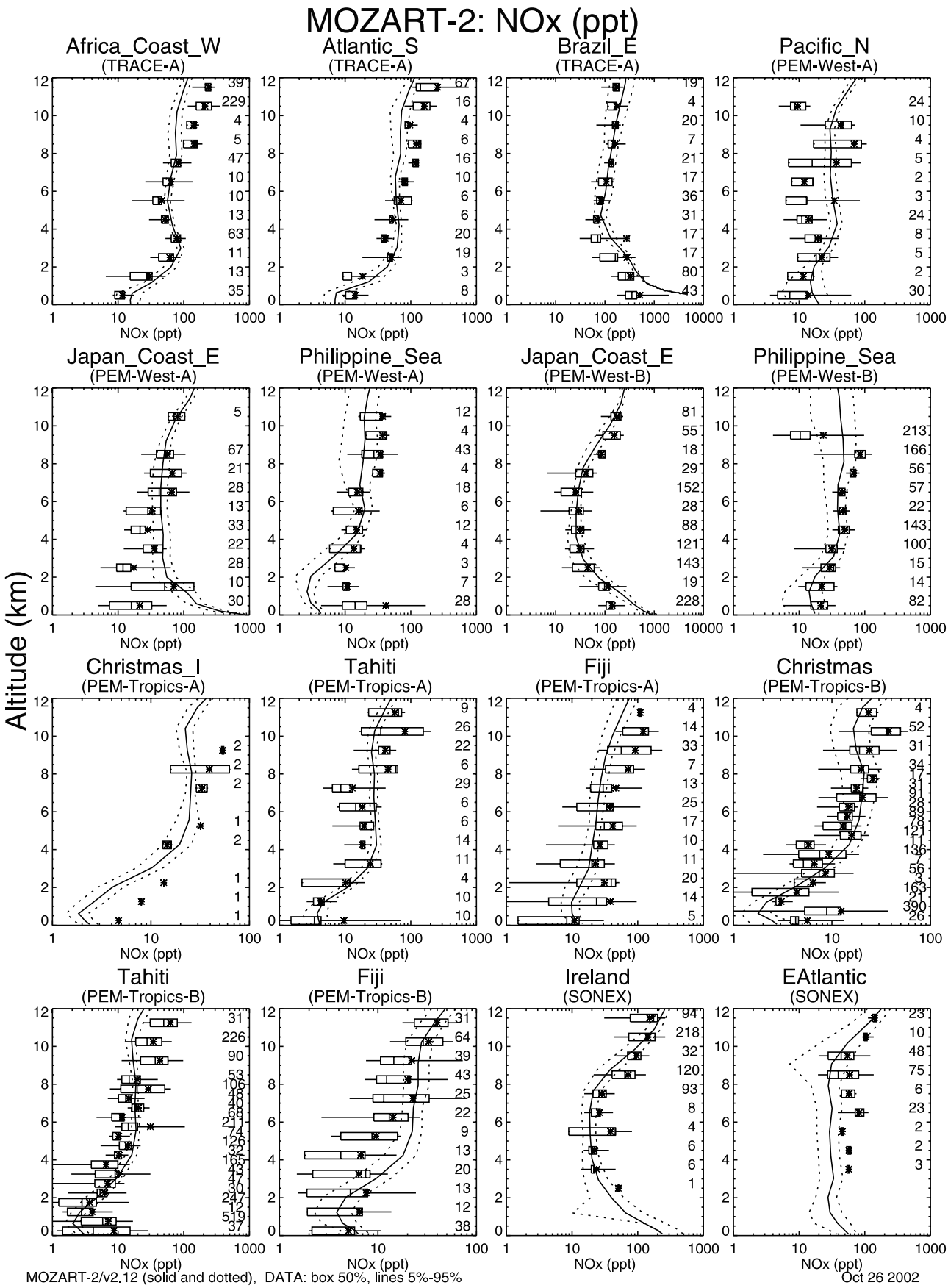
MOZART-2: NOx (ppt)
Africa_Coast_W
(TRACE-A)
Atlantic_S
(TRACE-A)
Brazil_E
(TRACE-A)
Pacific_N
(PEM-West-A)
Japan_Coast_E
(PEM-West-A)
Philippine_Sea
(PEM-West-A)
Japan_Coast_E
(PEM-West-B)
Philippine_Sea
(PEM-West-B)
Christmas_I
(PEM-Tropics-A)
Tahiti
(PEM-Tropics-A)
Fiji
(PEM-Tropics-A)
Christmas
(PEM-Tropics-B)
Tahiti
(PEM-Tropics-B)
Fiji
(PEM-Tropics-B)
Ireland
(SONEX)
EAtlantic
(SONEX)
Altitude (km)
NOx (ppt)
MOZART-2/v2.12 (solid and dotted), DATA: box 50%, lines 5%-95%
Oct 26 2002

middle latitudes (e.g., the PEM-West-A regions and Christmas Island in PEM-Tropics-A, and Tahiti and Fiji in PEM-Tropics-B), in which the model overestimates PAN concentrations in the upper troposphere by a factor of 2 (Figure 7). Note that these significant overestimates occur in regions in which the observed upper tropospheric PAN concentrations are quite low (typically <50 parts per trillion by volume (pptv)). The overestimate in these regions appears to result from convective transport of PAN precursors (including isoprene and its oxidation products) accompanied by NO_x from surface sources (biomass burning and soils) and lightning. This excessive production of PAN may indicate a problem with the parameterization of the lightning NO_x source, incorrect seasonality of biomass burning, or overly strong transport of PAN precursors to the upper troposphere by the *Zhang and McFarlane* [1995] convection scheme. The possibility of either poor seasonality of biomass burning or excessive convective transport is supported in some cases by comparisons of other species. For instance, MOZART also overestimates CO and C_3H_8 in the upper troposphere over Fiji during PEM-Tropics-B (see sections 3.3 and 3.4). In regions with higher observed PAN concentrations, by contrast, the model shows a somewhat better agreement with observations.

[24] Simulated concentrations of HNO_3 are in reasonable agreement with observations at most locations (Figure 8). The HNO_3 concentrations in MOZART-2 are highly sensitive to the parameterization of wet deposition. For instance, if we were to use much slower wet deposition rates for HNO_3 (e.g., by using the wet deposition formulation used by *Hauglustaine et al.* [1998] in MOZART-1), HNO_3 concentrations would be overestimated by a factor of 2 or more at most locations. The wet deposition fluxes of HNO_3 from MOZART-2 agree with the observations (compiled by *Dentener and Crutzen* [1994]) to within a factor of 2 at most stations (Figure 9). There is a significant systematic overestimate of wet deposition only for the South Asian region, where the model is generally high by more than a factor of 2. Many other current global three-dimensional models overestimate HNO_3 concentrations at many locations throughout the troposphere [e.g., *Hauglustaine et al.*, 1998; *Mickley et al.*, 1999; *Bey et al.*, 2001]. These studies generally attribute this overestimate to several causes, including inaccurate representation of wet deposition, neglecting partitioning of nitrate into the aerosol phase (whereas the observations include only the gas-phase nitric acid), and possible missing reactions to convert HNO_3 back to NO_x. We find no such systematic error in HNO_3 concentrations or wet deposition fluxes in MOZART-2.

3.3. Carbon Monoxide

[25] Monthly mean concentrations of CO predicted by the model are shown in Figure 10. High concentrations of CO are found near the surface over regions with large emissions from biomass burning or fossil fuel combustion. Over industrial regions, surface CO concentrations are highest during winter, reflecting the slow chemical loss and decreased ventilation of the boundary layer. During summer, OH concentrations increase dramatically, and background concentrations of CO over the ocean surface decrease considerably. In the tropics, the seasonality of CO concentrations also depends strongly on the seasonality of biomass burning, which accounts for over half of the direct emissions of CO.

[26] Surface CO-mixing ratios are compared with observations at selected measurement sites in Figure 11. Mean simulated CO concentrations agree well with observations at most of the observation sites, but there are discrepancies in the seasonal cycle at a number of locations. In the tropics, the simulated seasonal cycle agrees reasonably with observations at most sites (e.g., Mahe Island, Ascension Island), while there is a tendency for the simulated concentrations to be too low by 10 parts per billion by volume (ppbv) or more in some months. The seasonal maximum at Christmas Island is delayed by 3 months relative to the observations, possibly indicating a problem with the timing of biomass burning or a problem with transport in the model (such as a poorly located Intertropical Convergence Zone (ITCZ)). At the extratropical sites in the Southern Hemisphere, MOZART simulates the observed CO concentrations and seasonal cycle well. At several sites at high northern latitudes, including Alert and Barrow, the model underestimates the observed seasonal cycle, while simulating the mean concentration well. At some subtropical sites in the Northern Hemisphere, such as Canary Islands and Mauna Loa, the springtime peak present in the observations is too weak in the model. These weaknesses in the simulation of CO may reflect problems with the biomass burning seasonal cycle or may result from problems with the spatial or seasonal distribution of the OH in our model. A similar underestimation of the seasonal cycle at high northern latitudes by *Holloway et al.* [2000] was attributed to unrealistically strong downward transport from the lower stratosphere, insufficient mixing of CO from lower latitudes, and emissions of CO from fossil fuel combustion that were too low. *Bey et al.* [2001] noted that their model underestimated CO concentrations at most locations. MOZART-2 does not show such a global bias (except for the slight underestimate in the tropics), but the total direct emissions of CO in our model are about 25% higher than those used by *Bey et al.* [2001].

[27] Simulated CO profiles agree with observations to within 10 ppbv at most sites, and generally capture the observed vertical gradients (Figure 12). At a few locations, however, the model overestimates observations by more than 10 ppbv, (Hawaii, PEM-Tropics-A, not shown) or underestimates observations by more than 10 ppbv (Philippine Sea and Pacific_Tropics_W (not shown), PEM-West-A). Above, the model was shown to agree well with

Figure 6. (opposite) Mean observed (box-whisker) and simulated (solid and dotted lines) regional vertical profiles of NO_x (pptv). The region and field campaign names are given above each plot. Observations are from aircraft field campaigns (see Table 3 for listing of field campaigns and regions), as compiled by *Emmons et al.* [2000]. The observed values are shown as mean (star), median (vertical bar), central 50% of the data (box), and central 90% of the data (horizontal line). The simulated values are shown as mean (solid line) $\pm 1\sigma$ standard deviation (dotted lines). Note that in some field campaigns the reported observed NO_x concentration is computed as the sum of the observed NO concentration and the NO_2 concentration calculated by a box model [see *Emmons et al.*, 2000]. See color version of this figure in the HTML.

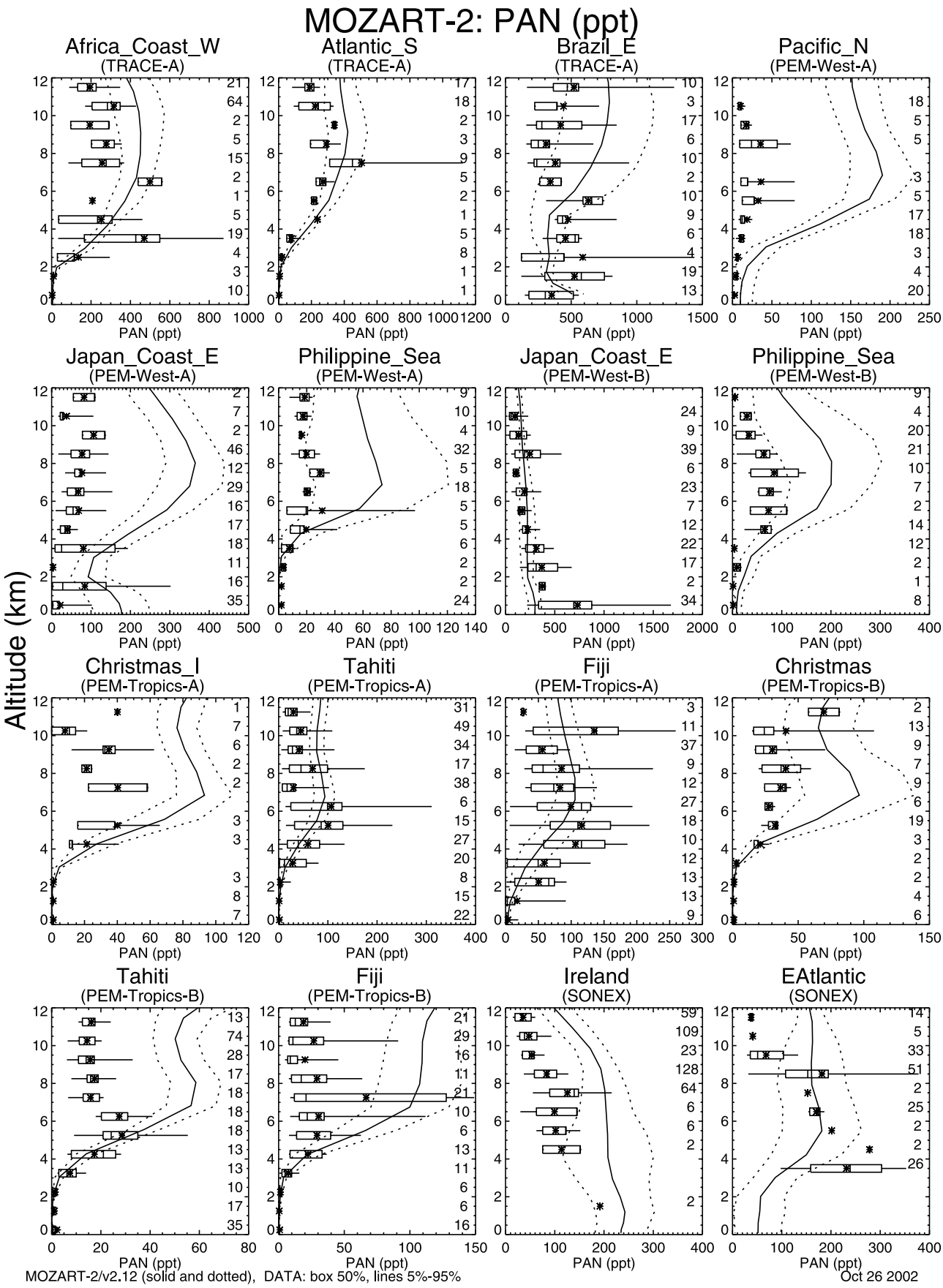

Figure 7. Same as Figure 6 but for PAN (pptv). See color version of this figure in the HTML.

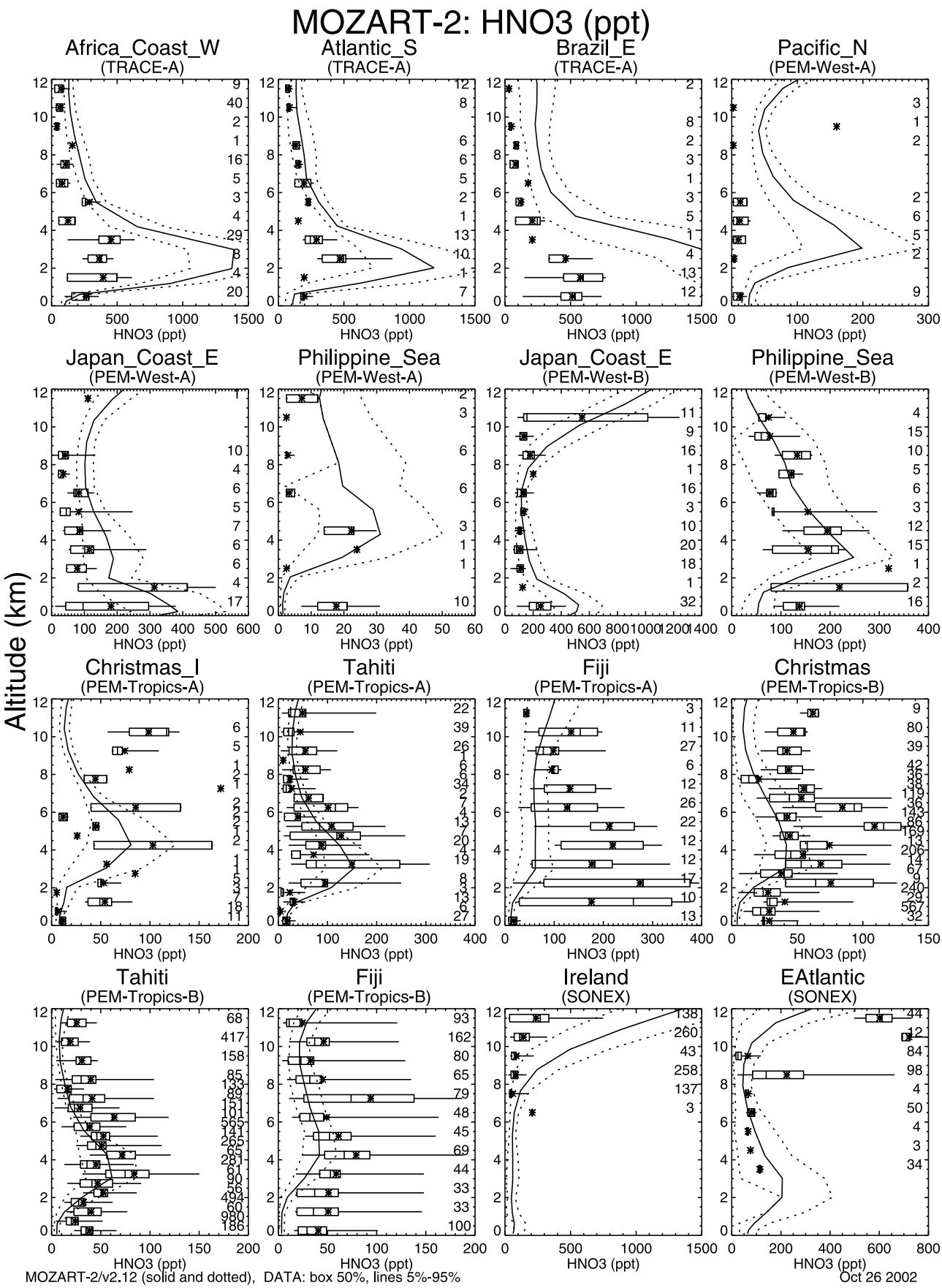

Figure 8. Same as Figure 6 but for HNO_3 (pptv). See color version of this figure in the HTML.

Table 3. Regions for Vertical Profiles of Aircraft Observations

Region Name	Expedition	Latitude	Longitude	Date
North Pacific	PEM-West-A	15°–35°N	180°–150°W	16 Sept. to 21 Oct. 1991
Japan coast, east	PEM-West-A	25°–40°N	135°–150°E	16 Sept. to 21 Oct. 1991
Phillipine Sea	PEM-West-A	5°–20°N	135°–150°E	16 Sept. to 21 Oct. 1991
Japan coast, east	PEM-West-B	25°–40°N	135°–150°E	7 Feb. to 14 March 1994
Phillipine Sea	PEM-West-B	5°–20°N	135°–150°E	7 Feb. to 14 March 1994
Africa coast, west	TRACE-A	25°–5°S	0°–10°E	21 Sept. to 26 Oct. 1992
South Atlantic	TRACE-A	20°S to equator	20°–10°W	21 Sept. to 26 Oct. 1992
Brazil, east	TRACE-A	15°–5°S	50°–40°W	21 Sept. to 26 Oct. 1992
Christmas Island	PEM-Tropics-A	equator to 10°N	160°–140°W	15 Aug. to 15 Oct. 1996
Tahiti	PEM-Tropics-A	20°S to equator	160°–130°W	15 Aug. to 15 Oct. 1996
Fiji	PEM-Tropics-A	30°–10°S	170°E–170°W	15 Aug. to 15 Oct. 1996
Christmas Island	PEM-Tropics-B	equator to 10°N	160°–140°W	6 March to 18 April 1999
Tahiti	PEM-Tropics-B	20°S to equator	160°–130°W	6 March to 18 April 1999
Fiji	PEM-Tropics-B	30°–10°S	170°E–170°W	6 March to 18 April 1999
East Atlantic	SONEX	35°–45°N	35°–15°W	7 Oct. to 12 Nov. 1997
Ireland	SONEX	50°–60°N	15°–5°W	7 Oct. to 12 Nov. 1997

CO at Mauna Loa, Hawaii, during the August–October season during which PEM-Tropics-A was conducted but to slightly underestimate the observations at Christmas Island during these months. However, the model overestimates the observations from PEM-Tropics-A over both of these regions (comparison with Hawaii region not shown). This may indicate atypical transport patterns or biomass burning emissions during the period of this campaign [e.g., *Staudt et al.*, 2002].

3.4. Nonmethane Hydrocarbons

[28] Simulated regional vertical profiles of the hydrocarbons ethane and propane are compared with observations in Figures S1 and S2 (auxiliary material), respectively. The model simulates observed mean concentrations for ethane to within ±25% at most locations. The model results for propane compare similarly well with observations. As with CO, however, the model underestimates concentrations of both these hydrocarbons in the Philippine Sea and Pacific_Tropics_W (not shown) regions (PEM-West-A). The simultaneous underestimate of CO and ethane and propane in these regions may indicate a missing emission source in or upwind of these regions, possibly too weak of an ocean source. Alternatively, a transport problem in the model could be causing inadequate transport of pollution to this region during the September–October period. There is also an underestimate of the alkanes in the East Atlantic region (Subsonic Assessment, Ozone and Nitrogen Oxide Experiment (SONEX)).

3.5. Oxygenated Species

[29] Formaldehyde is a key intermediate in the oxidation of methane and many NMHCs in the troposphere. Formaldehyde is lost primarily through photolysis and reaction with OH, with photolysis providing an important source of HO_x radicals in the troposphere. Comparisons between simulated and observed regional vertical profiles of formaldehyde are shown in Figure S3 (auxiliary material). In the regions with the most extensive observations, PEM-Tropics-B and some of the TRACE-A regions, the model simulates the observed concentrations of formaldehyde well. In other regions, e.g., Africa_Coast_W and Atlantic_S (TRACE-A), the model shows large disagreements with the observations. In these regions, however, the few available observations may not adequately represent the regional abundance of this short-lived species.

[30] Acetone has surface emissions from anthropogenic sources, biomass burning, and vegetation [*Jacob et al.*, 2002]. Observations made during PEM-Tropics-B indicated surprisingly large abundances of acetone over the tropical Pacific [*Singh et al.*, 2001], a region where most models predict quite low acetone concentrations [e.g., *Hauglustaine et al.*, 1998; *Bey et al.*, 2001]. These observations suggest the presence of a large natural, distributed source of oxygenated organic species [*Jacob et al.*, 2002]. Recent oceanic observations suggest that photochemical production of acetone may occur in the surface ocean [*Zhou and Mopper*, 1997]. We include a speculative oceanic source of acetone in our model. Acetone also has a large secondary source in the troposphere from oxidation of NMHCs, primarily propane. Acetone has a tropospheric lifetime ranging from less than a month to several months. Photolysis of acetone is an important source of HO_x radicals in the upper troposphere [*Jaeglé et al.*, 2001]. Vertical profiles of acetone from the model and observations are compared in Figure S4 (auxiliary material). In most of the regions (including those from the TRACE-A and SONEX campaigns, and some sites from PEM-West-B and PEM-Tropics-B), the model estimates of acetone agree reasonably well with observations. The inclusion of an ocean source of acetone in MOZART-2 improves the agreement between simulated and observed concentrations, but the model still underestimates acetone by up to a factor of 2 in the Tahiti and Easter Island (not shown) regions (PEM-Tropics-B). The ocean source also contributes to an overestimate of acetone in the lower troposphere at certain sites (e.g., Japan_Coast_E in PEM-West-B). A stronger oceanic source of acetone, as suggested by *Jacob et al.* [2002] (27 Tg yr^{-1}), may improve the agreement with observations in the regions where it is currently underestimated but was rejected in this study because it produced too large a vertical gradient of acetone over ocean sites and a larger overestimate of PAN concentrations in the upper troposphere (see section 3.2).

[31] Hydroperoxides are formed in the atmosphere by permutation reactions between peroxy radicals. Self-reaction of HO_2 forms H_2O_2, while reaction of CH_3O_2 with HO_2

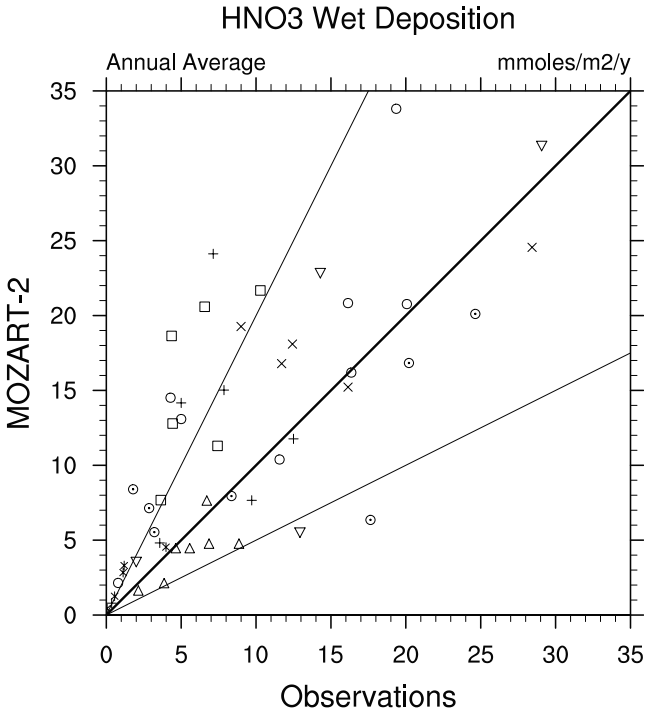

Figure 9. Comparison of observed and simulated annual wet deposition fluxes of HNO_3 (mmol m^{-2} yr^{-1}). Observations are compiled by *Dentener and Crutzen* [1994], and the site locations and fluxes are listed in Table V of that work. Plotting symbols are coded based on the location of the station: Europe (circled dot), South America (plus), North America (open circle), East Asia (cross), South Asia (square), Oceania (triangle), Africa (downward facing triangle), and others (asterisk). The thick line is the 1:1 line, and the thin lines are the 1:2 and 2:1. The zero-intercept reduced major axis regression line has a slope of 1.25, with a correlation coefficient of $r^2 = 0.81$. See color version of this figure in the HTML.

forms methylhydroperoxide (CH_3OOH). These reactions are the main sinks for HO_x radicals in much of the troposphere. Because of this coupling between HO_x radicals and hydroperoxides, evaluation of simulated concentrations of H_2O_2 and CH_3OOH provide an indirect test of the model simulation of HO_x. An important difference between H_2O_2 and CH_3OOH is the much higher solubility of H_2O_2, leading to more rapid removal by wet deposition. The weakly soluble CH_3OOH can be convected to the upper troposphere, where it may provide an important source of HO_x [*Prather and Jacob*, 1997]. Simulated concentrations of H_2O_2 and CH_3OOH are compared with observations in Figures S5 and S6 (auxiliary material), respectively. The model simulates observed concentrations and vertical gradients of these species very well in most regions. One exception is the overestimate of the hydroperoxides in the lower troposphere by more than a factor of 2 in the East Atlantic and Newfoundland (not shown) regions (SONEX). The model underestimates H_2O_2 by 20–50% in the lower troposphere in the Philippine Sea and Pacific_Tropics_W (not shown) regions during the PEM-West-A campaign; CH_3OOH is similarly underestimated by about 25% in these regions.

3.6. Hydroxyl Radical

[32] The OH is the primary oxidant in the troposphere and is responsible for the removal of many reduced compounds from the atmosphere. The zonally and monthly averaged distributions of OH are shown in Figure 13. Concentrations of OH are highest in the lower to middle troposphere in the tropics and in northern midlatitudes during summer. The simulated OH concentrations are similar to those computed by *Spivakovsky et al.* [2000], generally agreeing with those estimates at most locations and seasons to within 10–20%.

[33] The lifetime of long-lived gases, such as methane and methylchloroform (1,1,1-trichloroethane, CH_3CCl_3), versus reaction with tropospheric OH provides a measure of the overall abundance of OH in the troposphere, with an emphasis on the tropical lower troposphere, where the warm temperatures allow the reactions of these species with OH to proceed quickly [e.g., *Spivakovsky et al.*, 2000; *Lawrence et al.*, 2001]. In our model, the methane lifetime versus tropospheric OH (defined as the atmospheric methane burden divided by the annual sink of methane by reaction with OH in the troposphere) is 9.4 years. The total methane burden is 4630 Tg (tropospheric burden, 3930 Tg), and the tropospheric sink by reaction with OH is 495 Tg yr^{-1} (loss to OH in the stratosphere, 9 Tg yr^{-1}). The 2001 Intergovernmental Panel on Climate Change (IPCC) report [*Prather et al.*, 2001] estimated a sink versus tropospheric OH of 507 Tg yr^{-1}, with a corresponding lifetime of 9.6 years (total lifetime including other loss processes, 8.4 years). The methane lifetime in MOZART-2 is reasonably consistent with this estimate by IPCC. Since methylchloroform is not simulated in MOZART-2, we use a uniform atmospheric mixing ratio for the calculation of its lifetime. We find an atmospheric lifetime for methylchloroform with respect to oxidation by tropospheric OH of 5.7 years. This estimate is in good agreement with the values of 5.5 years found by *Spivakovsky et al.* [2000] (based on a total atmospheric lifetime of 4.6 years, an ocean sink with lifetime of 80 years, and a stratospheric sink with lifetime of 43 years) and 5.7 years found by *Prinn et al.* [1995] (based on a total atmospheric lifetime of 4.8 years). If we used a more realistic distribution for methylchloroform, with lower mixing ratios in the stratosphere, the calculated lifetime with respect to oxidation by tropospheric OH in MOZART-2 would be decreased, and would likely agree better with the estimate by *Spivakovsky et al.* [2000]. The agreement between estimates of the lifetimes of methane and methylchloroform with those derived from observations suggests that the global tropospheric abundance of OH in MOZART-2 is reasonable. The OH abundance in our model is quite sensitive to the wet deposition parameterization, which can remove odd-hydrogen reservoirs such as peroxides from the atmosphere and to the distribution of water vapor (input from MACCM3), which controls an important source of odd-hydrogen in the troposphere. The OH abundance is also sensitive to photolysis rates, which are computed in the model from a lookup table.

4. Species Budgets

4.1. Ozone

[34] The budget of tropospheric ozone in MOZART-2 is shown in Table 4. This budget is calculated for odd oxygen,

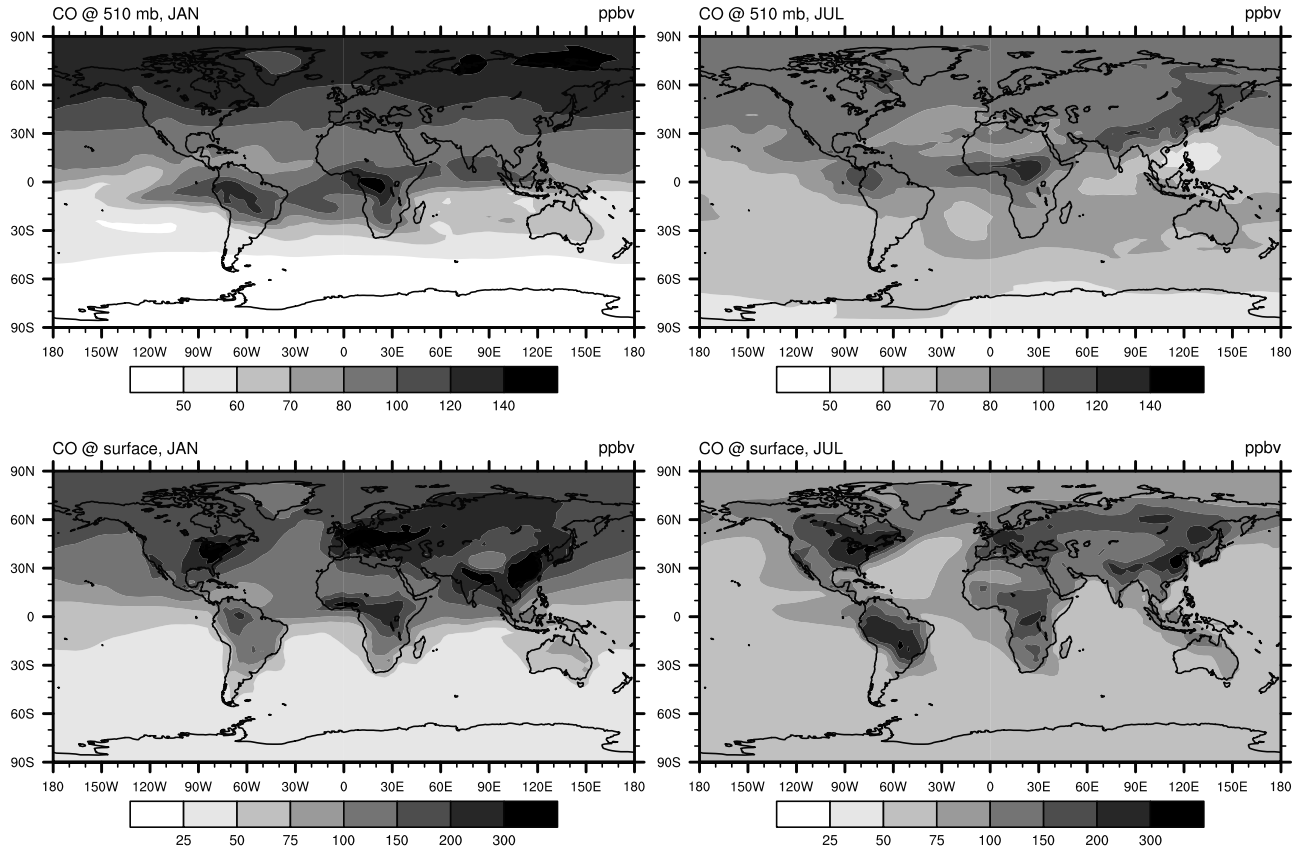

Figure 10. Same as Figure 2 but for CO (in ppbv). See color version of this figure at back of this issue.

defined as $O_x = O_3 + O(^1D) + O(^3P) + NO_2 + 2 \times NO_3 + 3 \times N_2O_5 + HO_2NO_2 + HNO_3 + PAN + MPAN$ to account for chemical recycling within this family of species. Ozone is the most abundant member of this chemical family, so the budget for O_x can be interpreted as a budget of ozone. Photochemical production of O_x results primarily from the reaction of NO with hydroperoxy radicals or organic peroxy radicals to form NO_2. The NO_2 photolyzes to form $O(^3P)$, which rapidly reacts with O_2 to form ozone. Photochemical loss of O_x occurs mainly through the reaction of $O(^1D)$ (from ozone photolysis) with H_2O to form 2 OH radicals, the reaction of ozone with OH and HO_2, and the ozonolysis of unsaturated hydrocarbons.

[35] The photochemical production and loss of ozone in the troposphere are estimated by MOZART to be 5258 and 4749 Tg yr^{-1}, respectively. These terms dominate over the net stratospheric input of 343 Tg yr^{-1}. The stratospheric input estimated by the model consists mostly of net advection of ozone across the tropopause (334 Tg yr^{-1}), with a small contribution from convection and vertical diffusion (9 Tg yr^{-1}). The loss of ozone by dry deposition at the surface is 857 Tg yr^{-1}. In an earlier version of MOZART-2, not using the LLNL pressure fixer, there was also a significant contribution (87 Tg yr^{-1}) to the tropospheric ozone budget resulting from mass consistency corrections in the advection scheme, as discussed in section 2.4 and in the work of *Jöckel et al.* [2001].

[36] The photochemical production and loss rates of ozone estimated here are much larger than the values obtained with MOZART-1 [*Hauglustaine et al.*, 1998; *Hauglustaine and Brasseur*, 2001]. These earlier studies only computed ozone budgets up to 250 hPa, while we extend the budget domain up to 100 hPa in the tropics. Even if we restrict the MOZART-2 budget domain to 250 hPa, the photochemical production and loss terms still exceed the values of *Hauglustaine and Brasseur* [2001] by 30 and 73%, respectively. The MOZART-1 production and loss rates, however, were quite low compared with estimates from other model simulations. The more rapid ozone photochemistry in MOZART-2 results in part from the inclusion of the *Zhang and McFarlane* [1995] deep convection scheme, which rapidly transports emitted species to the middle and upper troposphere increasing photochemical activity there, as well as from the 15% increase in total surface NO_x emissions. While, in general, inclusion of the *Zhang and McFarlane* [1995] scheme tends to improve model results, the vertical transport may be too strong, leading to excessive ozone production in the middle and upper troposphere in the northern extratropics. The ozone photochemical rates obtained in the present study fall approximately within the range obtained by recent studies, which is 3018–4900 Tg yr^{-1} for production, and 2511–4300 Tg yr^{-1} for loss [*Hauglustaine et al.*, 1998 and comparison therein; *Mickley et al.*, 1999; *Bey et al.*, 2001]. The ozone production and loss rates calculated are within 10% of those found by *Bey et al.* [2001]. Our stratospheric input value (343 Tg yr^{-1}) is below the range of recent modeling studies (390–846 Tg yr^{-1}) [*Hauglustaine et al.*, 1998 and comparison therein; *Mickley et al.*, 1999; *Bey et al.*, 2001] and the range recently

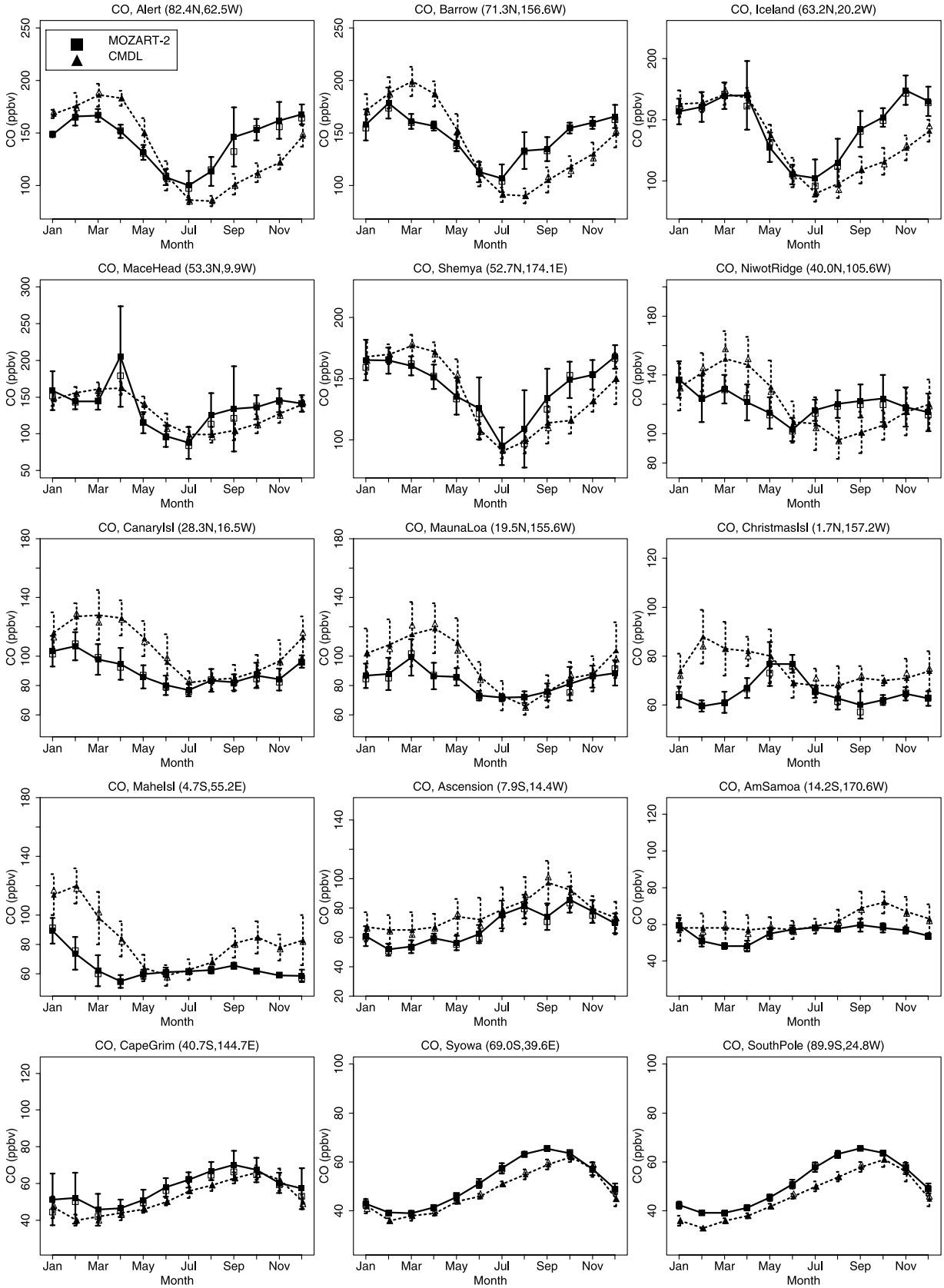

Figure 11. Comparison of observed (dotted lines) and simulated (solid lines) monthly mean carbon monoxide volume mixing ratios (ppbv) at surface sites. Observations are from the NOAA/CMDL flask measurement network [*Novelli et al.*, 1998]. Station names and locations (latitude and longitude) are given above each plot. Vertical bars indicate the standard deviations of the observations or model results within a month. See color version of this figure in the HTML.

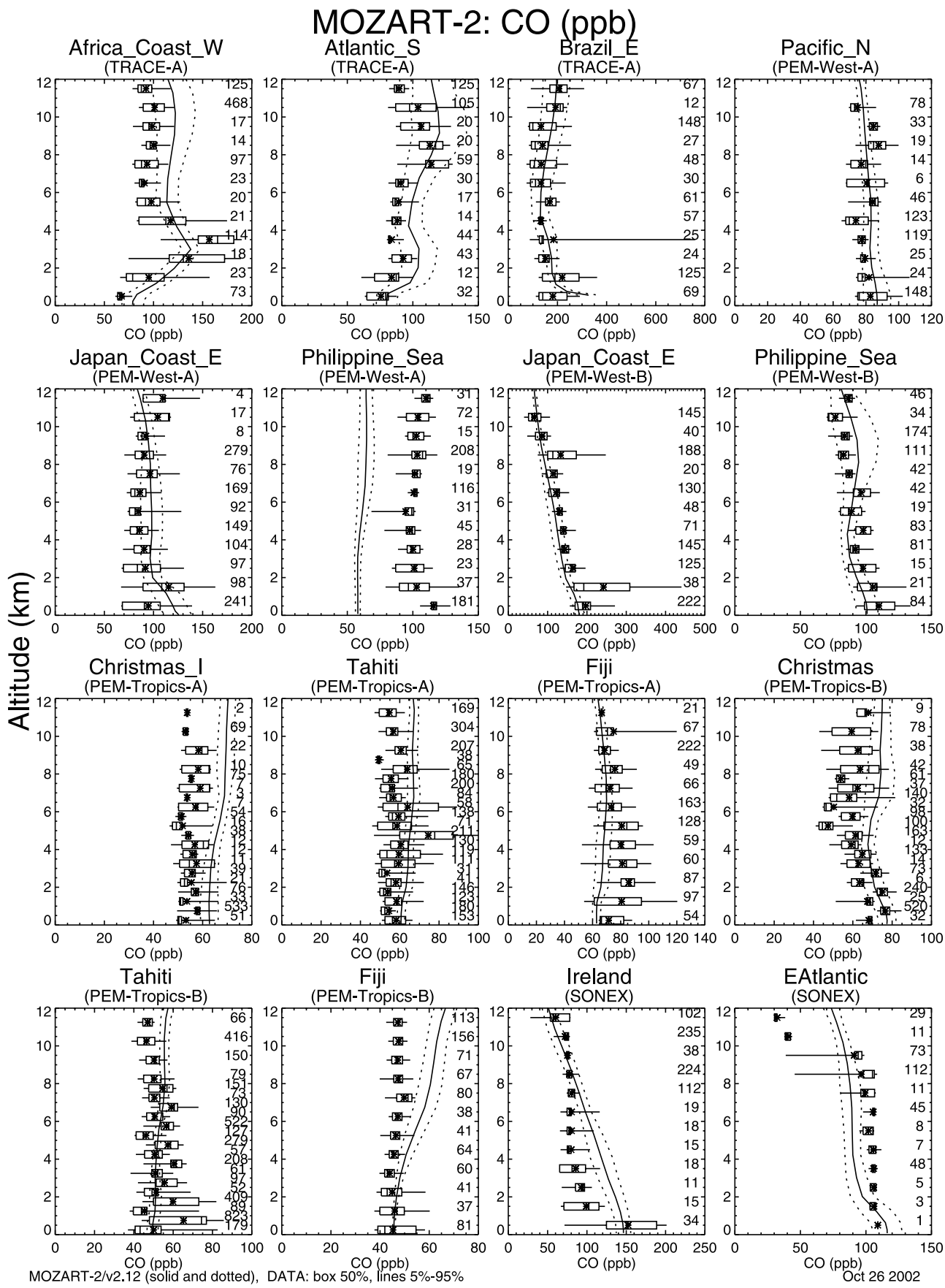

Figure 12. Same as Figure 6 but for CO (ppbv). See color version of this figure in the HTML.

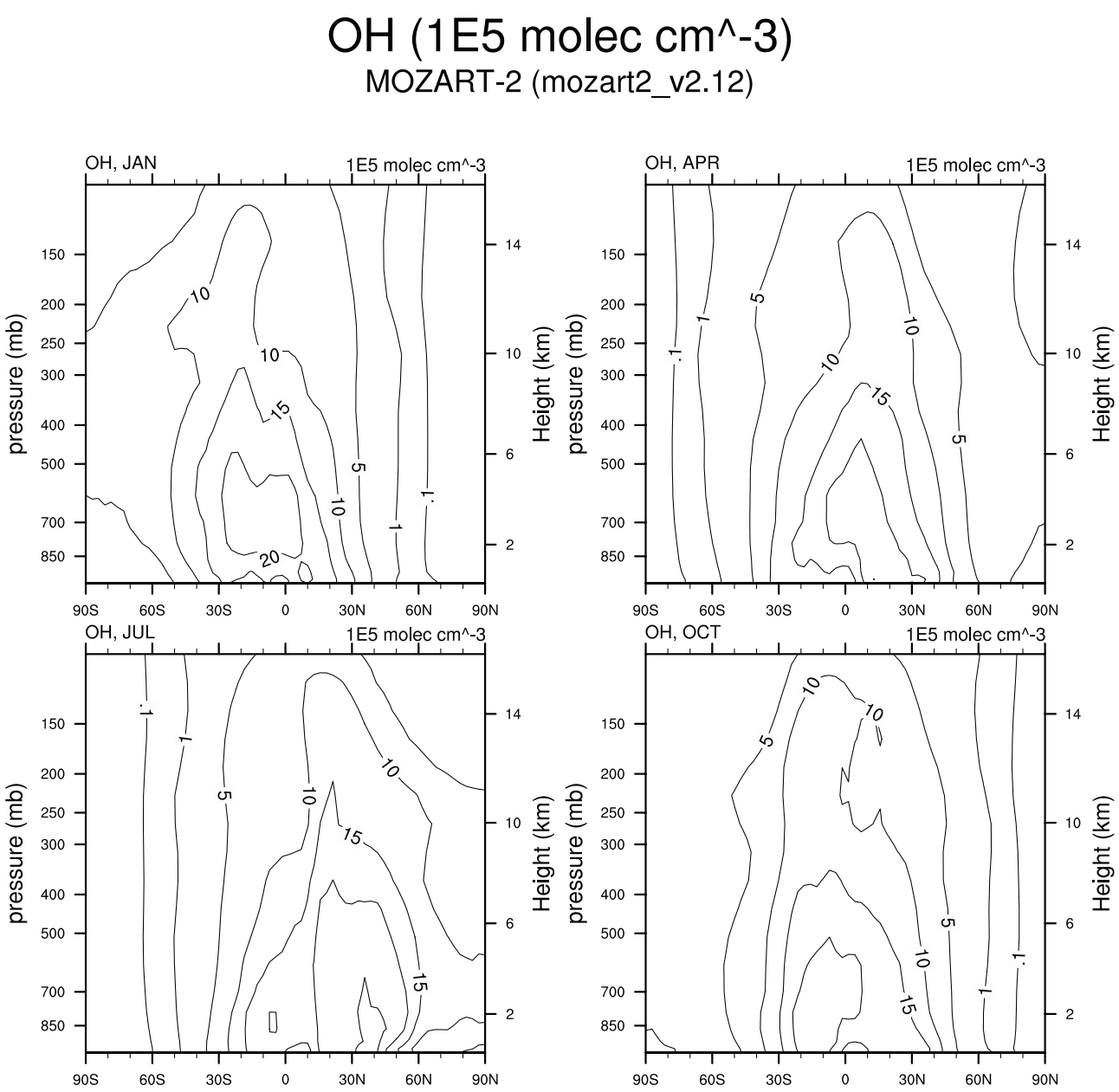

Figure 13. Zonally and monthly averaged concentrations of OH (in units of 10^5 molecules cm^{-3}) for January (upper left), April (upper right), July (lower left), and October (lower right).

Table 4. Annual Mean Budget of Tropospheric Ozone in MOZART-2[a]

	Source (Sink), Tg O_3 yr^{-1}					
Process	Global	Northern Hemisphere	Southern Hemisphere	Tropics	Northern Extratropics	Southern Extratropics
Influx from stratosphere[b]	343[c]	256	87	109	187	47
Photochemical production	5258	3178	2080	3951	1055	251
Photochemical loss	−4749	−2816	−1933	−3569	−868	−311
Dry deposition	−857	−583	−274	−458	−319	−80
Net tropospheric transport	0	−40	40	−32	−60	92
Burden, Tg O_3	362	203	159	203	99	60

[a]For this budget, the tropics are defined to extend from 30°S to 30°N, and the extratropics from 30° to 90°N or S. The tropopause is defined as the hybrid model level interface corresponding to approximately 100 hPa in the tropics and 250 hPa in the extratropics.
[b]Includes advection, convection, and vertical diffusion.
[c]This term consists of advection (334 Tg yr^{-1}) and convection and vertical diffusion (9 Tg yr^{-1}).

Table 5. Regional Production and Loss of Tropospheric Ozone in MOZART-2[a]

Production/Loss	Southern Extratropics	Tropics	Northern Extratropics	Total
Upper Troposphere (400 hPa to Tropopause)				
P	52	1005	105	1163
L	45	291	100	436
Middle Troposphere (700–400 hPa)				
P	99	1292	261	1653
L	143	1473	319	1936
Lower Troposphere (Surface to 700 hPa)				
P	100	1654	689	2442
L	123	1805	449	2377
Total (Surface to Tropopause)				
P	251	3951	1055	5258
L	311	3569	868	4749

[a]Values are given in Tg O_3 yr^{-1}. For this budget, the definitions of the tropics, extratropics, and tropopause are as in Table 4. The vertical regions used for this budget are defined to extend between the hybrid model level interfaces corresponding to the approximate pressures shown.

calculated by *McLinden et al.* [2000] based on measurements and tracer-tracer correlations (475 ± 120 Tg yr^{-1}).

[37] We also present in Table 4 the budgets of ozone in several geographical subdomains within MOZART-2, including the Northern and Southern Hemispheres, the tropics, and the northern and southern extratropics. We find a large hemispheric asymmetry in ozone production, with 53% more ozone being produced in the Northern Hemisphere. This asymmetry is even more pronounced if we consider only the extratropics, where the ozone production in the North is a factor of 4 larger than that in the South, reflecting the large difference in NO_x emissions in the two regions. We also find that more than half (54%) of the total stratosphere-troposphere exchange of ozone takes place in the northern extratropics, with the balance occurring in the tropics (32%) and the southern extratropics (14%). The values in Table 4 are sensitive to the definitions used for the regions. If, instead of the current definition, we chose to define the tropics as extending from 25°S to 25°N and the tropopause height as approximately 150 hPa in the tropics and 250 hPa in the extratropics, the total stratosphere-troposphere exchange would increase to 495 Tg yr^{-1}, partitioned as 66% in the northern extratropics, 0% in the tropics, and 34% in the southern extratropics.

[38] The vertical distribution of the chemical production and loss of ozone within the troposphere is shown in Table 5. The tropics are responsible for 75% of the total ozone production and loss, driven by large fluxes of UV radiation, high water vapor concentrations and temperatures, and biomass burning emissions and lightning. Within the tropics, production and loss are most rapid in the lower troposphere, accounting for 31 and 38%, respectively, of the global totals. The tropical middle troposphere is also a major contributor to production (25%) and loss (31%). In the tropical upper troposphere, gross production and loss rates are slower, but there is a large net production of ozone (714 Tg yr^{-1}) unlike the lower and middle troposphere in the tropics, where there is a net loss of ozone. Outside the tropics, the most active ozone chemistry is found in the Northern Hemisphere's lower troposphere. In this region, fueled by large anthropogenic NO_x emissions, 13% of the global production of tropospheric ozone occurs. There is also a significant net production of ozone (240 Tg yr^{-1}) in this region. Ozone chemistry becomes slower with increasing altitude in the northern extratropics. Ozone production and loss rates are smallest in the southern extratropics, with a small net loss occurring in both the lower and middle troposphere. Globally, the most rapid chemistry occurs in the lower troposphere, accounting for 46% of the gross ozone production and 50% of the loss in the troposphere. The upper troposphere has the strongest net production of ozone, while the middle troposphere is a region of net loss, and the lower troposphere is nearly in balance, with a small net production.

4.2. Carbon Monoxide

[39] The simulated budget for CO is shown in Table 6. Globally, the largest source of CO in the troposphere is in situ photochemical production from hydrocarbon oxidation. The other source of CO is direct emissions, the largest source of which is biomass burning. CO is lost from the troposphere almost exclusively by reaction with OH. The production and loss of CO occur primarily (over 75%) in the tropics. Net meridional transport of CO within the troposphere is from north to south. Large emissions of CO and precursor hydrocarbons in the northern extratropics, where CO has a relatively long lifetime versus oxidation by OH (averaging 2.4 months), lead to net export to the tropics, where the lifetime versus OH is much shorter (averaging 1.2 months). Large emissions of CO from biomass burning, together with large in situ production of CO, leads to a net export of CO from the tropics to the southern extratropics, where emissions and chemical production are quite low. The lifetime of CO versus oxidation by OH in the southern extratropics is longer than in any other region shown in Table 6, averaging 3.4 months. Local emissions and chemistry dominate over transport in the budget of CO in most of the regions shown in Table 6, due to the short lifetime of CO in the troposphere (∼1–3 months) relative to the meridional transport times between these regions. The most significant contribution by transport occurs in the southern extratropics, where transport from the tropics approximately equals the sum of emissions and photochemical production.

[40] Model studies of the CO budget have also been performed recently by *Hauglustaine et al.* [1998], *Granier et al.* [2000], *Holloway et al.* [2000], and *Bey et al.* [2001]. The direct surface emissions of CO in MOZART-2 (1195 Tg yr^{-1}) is within the range of 1043–1337 Tg yr^{-1} used in these other studies. The chemical production of CO in MOZART-2 (1545 Tg yr^{-1}) is slightly higher than the values of 1368 Tg yr^{-1} [*Granier et al.*, 2000] and 1443 Tg yr^{-1} [*Holloway et al.*, 2000], and much higher than the value found in MOZART-1 of 881 Tg yr^{-1} [*Hauglustaine et al.*, 1998]. The difference between MOZART-2 and MOZART-1 is due in part to higher production of CO from methane oxidation. The lifetime of methane in MOZART-2 versus tropospheric OH is ∼20% shorter than in MOZART-1, corresponding to a ∼25% increase in methane loss frequency; also, the tropospheric burden of methane is ∼10% greater in MOZART-2, due largely to the different domains over which the budgets were computed. Additionally, the production of CO from the oxidation of isoprene is larger in MOZART-2, as the biogenic emissions of isoprene are almost twice as large as the values used in MOZART-1.

Table 6. Annual Mean Budget of Tropospheric CO in MOZART-2[a]

Process	Source (Sink), Tg CO yr^{-1}					
	Global	Northern Hemisphere	Southern Hemisphere	Tropics	Northern Extratropics	Southern Extratropics
Emissions	1195	850	345	782	394	18
Flux from/to stratosphere	−39	−19	−20	28	−38	−30
Photochemical production	1545	867	678	1215	248	82
Photochemical loss	−2696	−1634	−1062	−2020	−501	−176
Dry deposition	−2	−2	0	−1	−2	0
Net tropospheric transport	0	−60	60	−4	−102	106
Burden, Tg CO	351	210	142	199	102	50

[a]For this budget, the definitions of the tropics, extratropics, and tropopause are as in Table 4.

We have also analyzed the continental-scale budgets in MOZART-2 for CO over Asia, the United States, and Europe; these budgets will be presented in a future paper (D. L. Mauzerall et al., manuscript in preparation, 2003).

5. Conclusions

[41] We have presented a new global chemical transport model for the troposphere, MOZART, version 2. The model, which includes 63 chemical species and 167 chemical and photochemical reactions, simulates the global distributions of ozone and its precursors, including NO_x, CO, and NMHCs. The model is an extension of version 1 of MOZART and is built on the framework of the NCAR MATCH transport model. It can be driven with a variety of meteorological inputs and is highly flexible in terms of spatial resolution and chemical mechanism. The version of MOZART-2 discussed in this paper uses meteorology from the NCAR MACCM3, and runs with a horizontal resolution of 2.8° latitude × 2.8° longitude with 34 hybrid vertical levels extending up to 4 hPa (approximately 40 km). The model can also be driven with assimilated meteorological fields, such as those provided by NCEP or ECMWF. Surface emissions in the model are based on up-to-date emission inventories and include sources from fossil fuel combustion, biofuel and biomass burning, biogenic and soil emissions, and oceanic emissions.

[42] The model is evaluated by thoroughly comparing simulation results with observations from ozonesondes, aircraft, and surface-monitoring stations. It successfully simulates the observed concentrations and seasonal cycle of ozone at most locations in the lower to middle troposphere. The agreement with observations of ozone is substantially improved compared with MOZART-1 [*Hauglustaine et al.*, 1998], in which tropospheric ozone was systematically too low, particularly at high latitudes and high altitudes. This improvement results from an improvement in the advection scheme, stronger convective transport, and improved chemical mechanism and emissions. There are still some disagreements between simulated ozone and observations. In particular, in the upper troposphere, at middle to high northern latitudes, the model tends to overestimate ozone in the vicinity of the tropopause by 25% or more at several sites. This may result from excessive downward transport of ozone from the stratosphere at these latitudes, inadequate resolution of the tropopause location, or excessive production of ozone in the upper troposphere.

[43] The tropospheric ozone production rate (∼5250 Tg yr^{-1}) and loss rate (∼4750 Tg yr^{-1}) dominate over the net stratospheric input rate (∼350 Tg yr^{-1}) and the loss by dry deposition (∼850 Tg yr^{-1}). These production and loss rates are on the high end of recent model studies, and are ∼30–85% higher than the values calculated in MOZART-1 [*Hauglustaine et al.*, 1998; *Hauglustaine and Brasseur*, 2001]. The chemical sources and sinks of ozone in the troposphere are dominated by the tropics, where 75% of the production and loss occurs. Production and loss rates of ozone are roughly 50% higher in the Northern Hemisphere than the Southern Hemisphere, with an even larger asymmetry in the extratropics. Net production of ozone within the troposphere occurs primarily in the tropical upper troposphere and the northern extratropical lower troposphere. Other regions are either roughly in photochemical balance or have a net loss of ozone. There is a strong hemispheric asymmetry in stratosphere-troposphere exchange of ozone; over half of the net influx of ozone occurs in the northern extratropics, a factor of 4 larger than occurs in the southern extratropics.

[44] The model simulates NO_x very well at almost all locations, over a range of concentrations spanning several orders of magnitude. The vertical profiles of PAN simulated by the model typically have a maximum in the middle to upper troposphere, in agreement with observations. However, the model tends to overestimate the magnitude of this peak in several regions in the tropics and subtropics, possibly due to excessive production of NO_x from lightning, poor seasonality of biomass burning, and overly strong convective transport of PAN precursors. Model concentrations and wet deposition fluxes of HNO_3 are in good agreement with observations. Concentrations of HNO_3 are not systematically biased high, as is the case for many recent global chemical transport model studies. HNO_3 concentrations are highly sensitive to the parameterization of wet deposition in the model.

[45] Simulations of carbon monoxide are generally in good agreement with surface and airborne observations. However, at some northern high-latitude stations, the model underestimates the CO seasonal cycle, while at some northern subtropical sites, the simulated springtime peak is too weak. These deficiencies may be due to problems with the seasonal cycle of biomass burning, or regional or seasonal errors in simulated OH concentrations. The emissions of CO used in this study are within the range of other recent studies, while the simulated photochemical production and loss rates are larger than those in most recent studies. In particular, the tropospheric production of CO is 75% higher than in MOZART-1 [*Hauglustaine et al.*, 1998], due in part to greater production from methane and iso-

prene. About 75% of the tropospheric production and loss of CO is found to occur within the tropics. Our simulation indicates net southward meridional transport of CO from the northern extratropics to the tropics, and from the tropics to the southern extratropics.

[46] The NMHCs ethane and propane agree with observations to within ±25% at most locations. The carbonyl species formaldehyde and acetone are also simulated well by the model, although acetone is underestimated in some remote tropical regions, even with the addition of an oceanic source. The concentrations and vertical profiles of the hydroperoxides, hydrogen peroxide, and methylhydroperoxide, agree well with observations in most regions.

[47] The concentration of OH, which determines the removal rate of many reduced species from the troposphere, in MOZART-2 agrees well with the recent estimates of the global OH distribution by *Spivakovsky et al.* [2000] and of the lifetime of methane [*Prather et al.*, 2001] and methylchloroform [*Prinn et al.*, 1995; *Spivakovsky et al.*, 2000]. The OH abundance is sensitive to assumptions in the wet deposition scheme used in MOZART, as well as to the water vapor distribution and photolysis rates.

[48] MOZART-2 provides a good overall simulation of the distributions of key species in tropospheric chemistry, including ozone and its key precursors. Future versions of the model will address several remaining problems in the simulation, including the overestimate of O_3 and PAN in some regions of the upper troposphere. MOZART-2 will be made available for download from the Atmospheric Chemistry Division at NCAR (http://acd.ucar.edu/models/MOZART/), along with the necessary input data files and documentation.

[49] **Acknowledgments.** We thank our colleagues D. Hauglustaine, D. Kinnison, J.-F. Müller, and F. Sassi for their help throughout the process of developing and evaluating the model. In addition, we would like to thank D. Rotman, P. Cameron-Smith, and others at LNLL for useful discussions about the model, and for providing us with the code for their pressure fixer. This work also benefited from discussions with and assistance in evaluating the model from M. Newchurch, and D. Wuebbles and his group at UIUC. We thank H. Levy and W. Moxim for their helpful comments on the manuscript. The work of D. Mauzerall was supported by NASA-ACMAP grant NAG5-9810. L. Emmons was supported by NASA Interagency Agreement L-9301. The National Center for Atmospheric Research is operated by the University Corporation for Atmospheric Research under sponsorship of the National Science Foundation.

References

Andreae, M. O., and P. Merlet, Emission of trace gases and aerosols from biomass burning, *Global Biogeochem. Cycles*, *15*, 955–966, 2001.

Bey, I., D. J. Jacob, R. M. Yantosca, J. A. Logan, B. D. Field, A. M. Fiore, Q. Li, H. Y. Liu, L. J. Mickley, and M. G. Schultz, Global modeling of tropospheric chemistry with assimilated meteorology: Model description and evaluation, *J. Geophys. Res.*, *106*, 23,073–23,095, 2001.

Brasseur, G. P., X. X. Tie, P. J. Rasch, and F. Lefèvre, A three-dimensional simulation of the Antarctic ozone hole: Impact of anthropogenic chlorine on the lower stratosphere and upper troposphere, *J. Geophys. Res.*, *102*, 8909–8930, 1997.

Brasseur, G. P., D. A. Hauglustaine, S. Walters, P. J. Rasch, J.-F. Müller, C. Granier, and X. X. Tie, MOZART, a global chemical transport model for ozone and related chemical tracers: 1. Model description, *J. Geophys. Res.*, *103*, 28,265–28,289, 1998.

Brocheton, F., Representation des emissions anthropiques dans les modeles de chimie-transport: Sensibilite a la representation spatiale des emissions et au degre de raffinement du schema chimique, Ph.D. dissertation, Univ. Paris XII, Val de Marne, 1999.

DeFries, R. S., and J. R. G. Townshend, NDVI-derived land cover classification at global scales, *Int. J. Remote Sens.*, *15*, 3567–3586, 1994.

Dentener, F. J., and P. J. Crutzen, A three-dimensional model of the global ammonia cycle, *J. Atmos. Chem.*, *19*, 331–369, 1994.

Emmons, L. K., D. A. Hauglustaine, J.-F. Müller, M. A. Carroll, G. P. Brasseur, D. Brunner, J. Staehelin, V. Thouret, and A. Marenco, Data composites of airborne observations of tropospheric ozone and its precursors, *J. Geophys. Res.*, *105*, 20,497–20,538, 2000.

Emmons, L., et al., The budget of tropospheric ozone during TOPSE from two chemical transport models, *J. Geophys. Res.*, *108*(D8), 8372, doi:10.1029/2002JD002665, 2003.

Friedl, R., (Ed.), Atmospheric effects of subsonic aircraft: Interim assessment report of the advanced subsonic technology program, *NASA Ref. Publ.*, *1400*, 143 pp., 1997.

Giorgi, F., and W. L. Chameides, The rainout parameterization in a photochemical model, *J. Geophys. Res.*, *90*, 7872–7880, 1985.

Granier, C., G. Pétron, J.-F. Müller, and G. Brasseur, The impact of natural and anthropogenic hydrocarbons on the tropospheric budget of carbon monoxide, *Atmos. Environ.*, *34*, 5255–5270, 2000.

Guenther, A., et al., A global model of natural volatile organic compound emissions, *J. Geophys. Res.*, *100*, 8873–8892, 1995.

Guenther, A., C. Geron, T. Pierce, B. Lamb, P. Harley, and R. Fall, Natural emissions of non-methane volatile organic compounds, carbon monoxide, and oxides of nitrogen from North America, *Atmos. Environ.*, *34*, 2205–2230, 2000.

Hack, J. J., Parameterization of moist convection in the NCAR community climate model (CCM2), *J. Geophys. Res.*, *99*, 5551–5568, 1994.

Hansen, J., M. Sato, and R. Ruedy, Radiative forcing and climate response, *J. Geophys. Res.*, *102*, 6831–6864, 1997.

Hao, W. M., and M.-H. Liu, Spatial and temporal distribution of tropical biomass burning, *Global Biogeochem. Cycles*, *8*, 495–503, 1994.

Hauglustaine, D. A., and G. P. Brasseur, Evolution of tropospheric ozone under anthropogenic activities and associated radiative forcing of climate, *J. Geophys. Res.*, *106*, 32,337–32,360, 2001.

Hauglustaine, D. A., G. P. Brasseur, S. Walters, P. J. Rasch, J.-F. Müller, L. K. Emmons, and M. A. Carroll, MOZART, a global chemical transport model for ozone and related chemical tracers: 2. Model results and evaluation, *J. Geophys. Res.*, *103*, 28,291–28,335, 1998.

Hess, P. G., S. Flocke, J.-F. Lamarque, M. C. Barth, and S. Madronich, Episodic modeling of the chemical structure of the troposphere as revealed duing the spring MLOPEX 2 intensive, *J. Geophys. Res.*, *105*, 26,809–26,839, 2000.

Holloway, T., H. Levy II, and P. Kasibhatla, Global distribution of carbon monoxide, *J. Geophys. Res.*, *105*, 12,123–12,147, 2000.

Holtslag, A., and B. Boville, Local versus nonlocal boundary-layer diffusion in a global climate model, *J. Clim.*, *6*, 1825–1842, 1993.

Horowitz, L. W., J. Liang, G. M. Gardner, and D. J. Jacob, Export of reactive nitrogen from North America during summertime: Sensitivity to hydrocarbon chemistry, *J. Geophys. Res.*, *103*, 13,451–13,476, 1998.

Jacob, D. J., B. D. Field, E. Jin, I. Bey, Q. Li, J. A. Logan, R. M. Yantosca, and H. B. Singh, Atmospheric budget of acetone, *J. Geophys. Res.*, *107*(D10), 4100, doi:10.1029/2001JD000694, 2002.

Jaeglé, L., D. J. Jacob, W. H. Brune, and P. O. Wennberg, Chemistry of HO*x* radicals in the upper troposphere, *Atmos. Environ.*, *35*, 469–489, 2001.

Jöckel, P., R. von Kuhlmann, M. G. Lawrence, B. Steil, C. A. M. Brenninkmeijer, P. J. Crutzen, P. J. Rasch, and B. Eaton, On a fundamental problem in implementing flux-form advection schemes for tracer transport in 3-dimensional general circulation and chemistry transport models, *Q. J. R. Meteorol. Soc.*, *127*, 1035–1052, 2001.

Kiehl, J. T., J. J. Hack, G. B. Bonan, B. A. Boville, D. L. Williamson, and P. J. Rasch, The National Center for Atmospheric Research Community Climate Model: CCM3, *J. Clim.*, *11*, 1131–1149, 1998.

Klinger, L. F., J. Greenberg, A. Guenther, G. Tyndall, P. Zimmerman, M. M'Bangui, J.-M. Moutsamboté, and D. Kenfack, Patterns in volatile organic compound emissions along a savanna-rainforest gradient in central Africa, *J. Geophys. Res.*, *103*, 1443–1454, 1998.

Lawrence, M. G., P. J. Crutzen, P. J. Rasch, B. E. Eaton, and N. M. Mahowald, A model for studies of tropospheric photochemistry: Description, global distributions, and evaluation, *J. Geophys. Res.*, *104*, 26,245–26,277, 1999.

Lawrence, M. G., P. Jöckel, and R. von Kuhlmann, What does the global mean OH concentration tell us?, *Atmos. Chem. Phys.*, *1*, 37–49, 2001.

Lelieveld, J., and F. J. Dentener, What controls tropospheric ozone?, *J. Geophys. Res.*, *105*, 3531–3551, 2000.

Levy, H., II, W. J. Moxim, and P. S. Kasibhatla, A global three-dimensional time-dependent lightning source of tropospheric NO_x, *J. Geophys. Res.*, *101*, 22,911–22,922, 1996.

Levy, H., II, W. J. Moxim, A. A. Klonecki, and P. S. Kasibhatla, Simulated tropospheric NO_x: Its evaluation, global distribution and individual source contributions, *J. Geophys. Res.*, *104*, 26,279–26,306, 1999.

Lin, S.-J., and R. B. Rood, Multidimensional flux-form semi-lagrangian transport schemes, *Mon. Weather Rev.*, *124*, 2046–2070, 1996.

Logan, J. A., An analysis of ozonesonde data for the troposphere: Recommendations for testing 3-D models and development of a gridded climatology for tropospheric ozone, *J. Geophys. Res.*, *104*, 16,115–16,149, 1999.

Logan, J. A., M. J. Prather, S. C. Wofsy, and M. B. McElroy, Tropospheric chemistry: A global perspective, *J. Geophys. Res.*, *86*, 7210–7254, 1981.

Madronich, S., and S. Flocke, The role of solar radiation in atmospheric chemistry, in *Handbook of Environmental Chemistry*, edited by P. Boule, pp. 1–26, Springer-Verlag, New York, 1998.

McLinden, C. A., S. C. Olsen, B. Hannegan, O. Wild, M. J. Prather, and J. Sundet, Stratospheric ozone in 3-D models: A simple chemistry and the cross-tropopause flux, *J. Geophys. Res.*, *105*, 14,653–14,665, 2000.

Mickley, L. J., P. P. Murti, D. J. Jacob, J. A. Logan, D. Rind, and D. Koch, Radiative forcing from tropospheric ozone calculated with a unified chemistry-climate model, *J. Geophys. Res.*, *104*, 30,153–30,172, 1999.

Moxim, W. J., and H. Levy II, A model analysis of the tropical South Atlantic Ocean tropospheric ozone maximum: The interaction of transport and chemistry, *J. Geophys. Res.*, *105*, 17,393–17,415, 2000.

Müller, J.-F., Geographical distribution and seasonal variation of surface emissions and deposition velocities of atmospheric trace gases, *J. Geophys. Res.*, *97*, 3787–3804, 1992.

Müller, J.-F., and G. Brasseur, IMAGES: A three-dimensional chemical transport model of the global troposphere, *J. Geophys. Res.*, *100*, 16,445–16,490, 1995.

National Research Council (NRC), *Rethinking the Ozone Problem in Urban and Regional Air Pollution*, Natl. Acad. Press, Washington, D. C., 1991.

Novelli, P. C., K. A. Masarie, and P. M. Lang, Distributions and recent changes of carbon monoxide in the lower troposphere, *J. Geophys. Res.*, *103*, 19,015–19,033, 1998.

Olivier, J. G. J., and J. J. M. Berdowski, Global emission sources and sinks, in *The Climate System*, edited by J. Berdowski, R. Guicherit, and B. J. Heij, pp. 33–77, Swets & Zeitlinger, Lisse, Netherlands, 2001.

Olivier, J. G. J., A. F. Bouwman, C. W. M. van der Maas, J. J. M. Berdowski, C. Veldt, J. P. J. Bloos, A. J. H. Visschedijk, P. Y. J. Zandveld, and J. L. Haverlag, Description of EDGAR version 2.0: A set of global emission inventories of greenhouse gases and ozone-depleting substances for all anthropogenic and most natural sources on a per country basis and on a 1×1 degree grid, *RIVM Rep. 771060 002/TNO-MEP Rep. R96/119*, Natl. Inst. of Public Health and Environ., Bilthoven, Netherlands, 1996.

Orlando, J. J., G. S. Tyndall, and S. E. Paulson, Mechanism of the OH-initiated oxidation of methacrolein, *Geophys. Res. Lett.*, *26*, 2191–2194, 1999.

Pickering, K. E., Y. Wang, W.-K. Tao, C. Price, and J.-F. Müller, Vertical distributions of lightning NO_x for use in regional and global chemical transport models, *J. Geophys. Res.*, *103*, 31,203–31,216, 1998.

Prather, M. J., and D. J. Jacob, A persistent imbalance in HO_x and NO_x photochemistry of the upper troposphere driven by deep tropical convection, *Geophys. Res. Lett.*, *24*, 3189–3192, 1997.

Prather, M., et al., Atmospheric chemistry and greenhouse gases, in *Climate Change 2001: The Scientific Basis. Contribution of Working Group I to the Third Assessment Report of the Intergovernmental Panel on Climate Change*, edited by J. T. Houghton et al., pp. 239–287, Cambridge Univ. Press, New York, 2001.

Price, C., J. Penner, and M. Prather, NO_x from lightning, 1, Global distribution based on lightning physics, *J. Geophys. Res.*, *102*, 5929–5941, 1997.

Prinn, R. G., R. F. Weiss, B. R. Miller, J. Huang, F. N. Alyea, D. M. Cunnold, P. J. Fraser, D. E. Hartley, and P. G. Simmonds, Atmospheric trends and lifetime of CH_3CCl_3 and global OH concentrations, *Science*, *269*, 187–192, 1995.

Randel, W. J., F. Wu, J. M. Russell III, A. Roche, and J. Waters, Seasonal cycles and QBO variations in stratospheric CH_4 and H_2O observed in UARS HALOE data, *J. Atmos. Sci.*, *55*, 163–185, 1998.

Rasch, P. J., N. M. Mahowald, and B. E. Eaton, Representations of transport, convection, and the hydrologic cycle in chemical transport models: Implications for the modeling of short-lived and soluble species, *J. Geophys. Res.*, *102*, 28,127–28,138, 1997.

Sander, S. P., et al., Chemical kinetics and photochemical data for use in stratospheric modeling, supplement to Evalulation 12: Update of key reactions, *JPL Publ., 00-3*, 2000.

Singh, H., Y. Chen, A. Staudt, D. Jacob, D. Blake, B. Heikes, and J. Snow, Evidence from the Pacific troposphere for large global sources of oxygenated organic compounds, *Nature*, *410*, 1078–1081, 2001.

Spivakovsky, C. M., et al., Three-dimensional climatological distribution of tropospheric OH: Update and evaluation, *J. Geophys. Res.*, *105*, 8931–8980, 2000.

Staudt, A. C., D. J. Jacob, J. A. Logan, D. Bachiochi, T. N. Krishnamurti, and N. Poisson, Global chemical model analysis of biomass burning and lightning influences over the South Pacific in austral spring, *J. Geophys. Res.*, *107*(D14), 4200, doi:10.1029/2000JD000296, 2002.

Tie, X., G. Brasseur, L. Emmons, L. Horowitz, and D. Kinnison, Effects of aerosols on tropospheric oxidants: A global model study, *J. Geophys. Res.*, *106*, 22,931–22,964, 2001.

Tie, X., et al., Effect of sulfate aerosol on tropospheric NO_x and ozone budgets: Model simulations and TOPSE evidence, *J. Geophys. Res.*, *108*(D4), 8364, doi:10.1029/2001JD001508, 2003.

Tyndall, G. S., R. A. Cox, C. Granier, R. Lesclaux, G. K. Moortgat, M. J. Pilling, A. R. Ravishankara, and T. J. Wallington, Atmospheric chemistry of small organic peroxy radicals, *J. Geophys. Res.*, *106*, 12,157–12,182, 2001.

Wang, Y., D. J. Jacob, and J. A. Logan, Global simulation of tropospheric O_3-NO_x-hydrocarbon chemistry: 1. Model formulation, *J. Geophys. Res.*, *103*, 10,713–10,725, 1998a.

Wang, Y., J. A. Logan, and D. J. Jacob, Global simulation of tropospheric O_3-NO_x-hydrocarbon chemistry: 2. Model evaluation and global ozone budget, *J. Geophys. Res.*, *103*, 10,727–10,755, 1998b.

Wang, Y., D. J. Jacob, and J. A. Logan, Global simulation of tropospheric O_3-NO_x-hydrocarbon chemistry: 3. Origin of tropospheric ozone and effects of nonmethane hydrocarbons, *J. Geophys. Res.*, *103*, 10,757–10,767, 1998c.

Wesely, M. L., Parameterization of surface resistance to gaseous dry deposition in regional-scale numerical models, *Atmos. Environ.*, *23*, 1293–1304, 1989.

Yienger, J. J., and H. Levy II, Empirical model of global soil-biogenic NO_x emissions, *J. Geophys. Res.*, *100*, 11,447–11,464, 1995.

Zhang, G. J., and N. A. McFarlane, Sensitivity of climate simulations to the parameterization of cumulus convection in the Canadian climate centre general circulation model, *Atmos. Ocean*, *33*, 407–446, 1995.

Zhou, X. L., and K. Mopper, Photochemical production of low-molecular-weight carbonyl compounds in seawater and surface microlayer and their air-sea exchange, *Mar. Chem.*, *56*, 201–213, 1997.

G. P. Brasseur and M. G. Schultz, Max Planck Institute for Meteorology, Bundestraße 55, D-20146 Hamburg, Germany. (brasseur@dkrz.de; martin.schultz@dkrz.de)

L. K. Emmons, J.-F. Lamarque, J. J. Orlando, P. J. Rasch, X. Tie, G. S. Tyndall, and S. Walters, National Center for Atmospheric Research, 1850 Table Mesa Drive, Boulder, CO 80303, USA. (emmons@ucar.edu; lamar@ncar.ucar.edu; orlando@acd.ucar.edu; pjr@ucar.edu; xxtie@ucar.edu; tyndall@acd.ucar.edu; stacy@acd.ucar.edu)

C. Granier, Service d'Aeronomie, University of Paris, Tour 15-14; 5eme etage, Boite 102, 4 Place Jussieu, F-75005 Paris, France. (clg@aero.jussieu.fr)

L. W. Horowitz, Geophysical Fluid Dynamics Laboratory, NOAA, Princeton University, P.O. Box 308, Princeton, NJ 08542, USA. (larry.horowitz@noaa.gov)

D. L. Mauzerall, Woodrow Wilson School, Princeton University, 406 Robertson Hall, Princeton, NJ 08544-1013, USA. (mauzeral@princeton.edu)

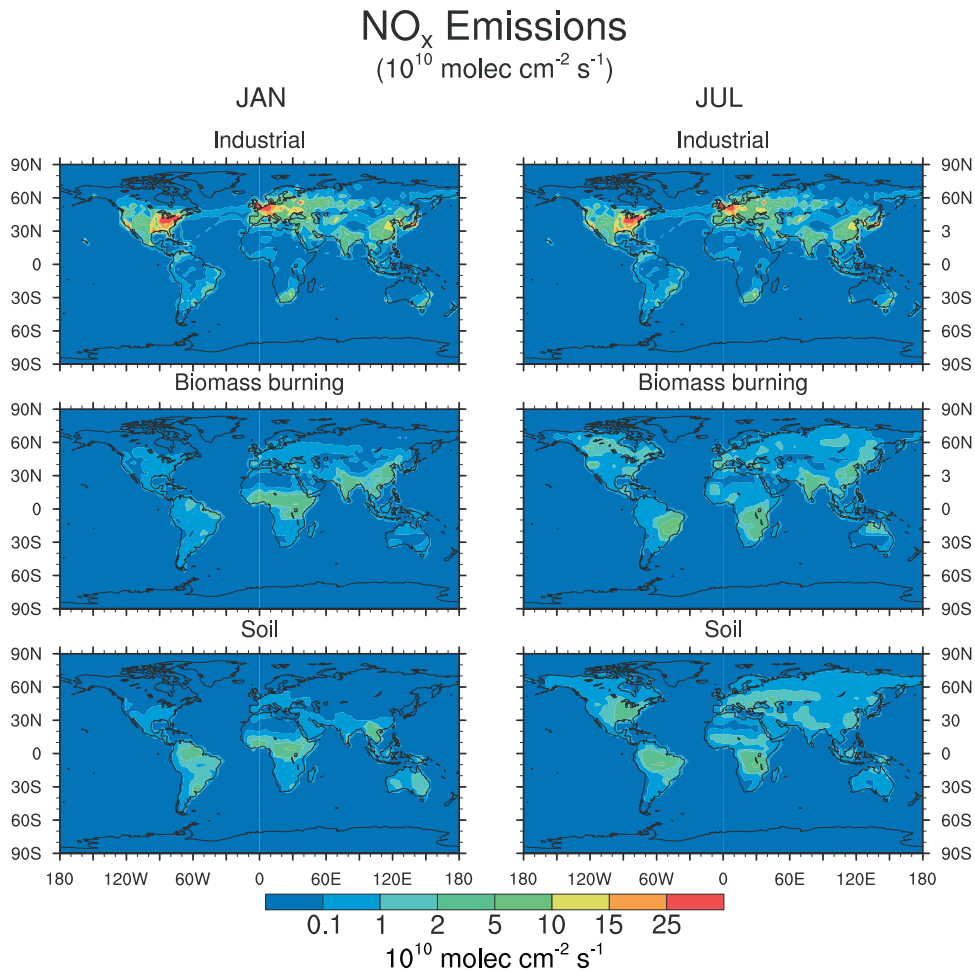

Figure 1. Monthly mean surface emissions (in units of 10^{10} molecules cm^{-2} s^{-1}) of nitrogen oxides (as NO) from industrial sources (top), biomass and biofuel burning (middle), and biogenic emissions from soil (bottom) for January (left) and July (right).

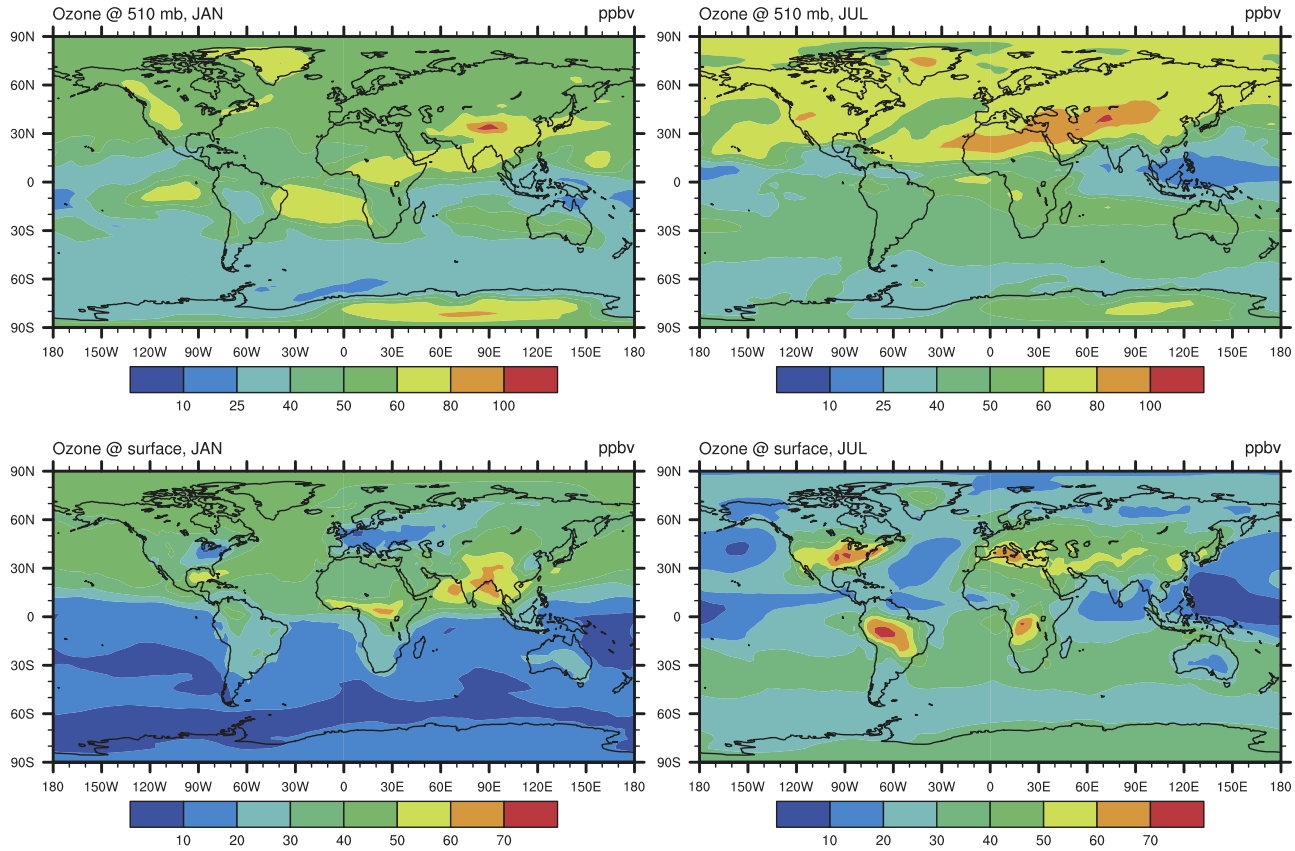

Figure 2. Monthly mean simulated concentrations of ozone (in ppbv) in January (left) and July (right) at hybrid model levels corresponding approximately to 970 (bottom) and 510 hPa (top).

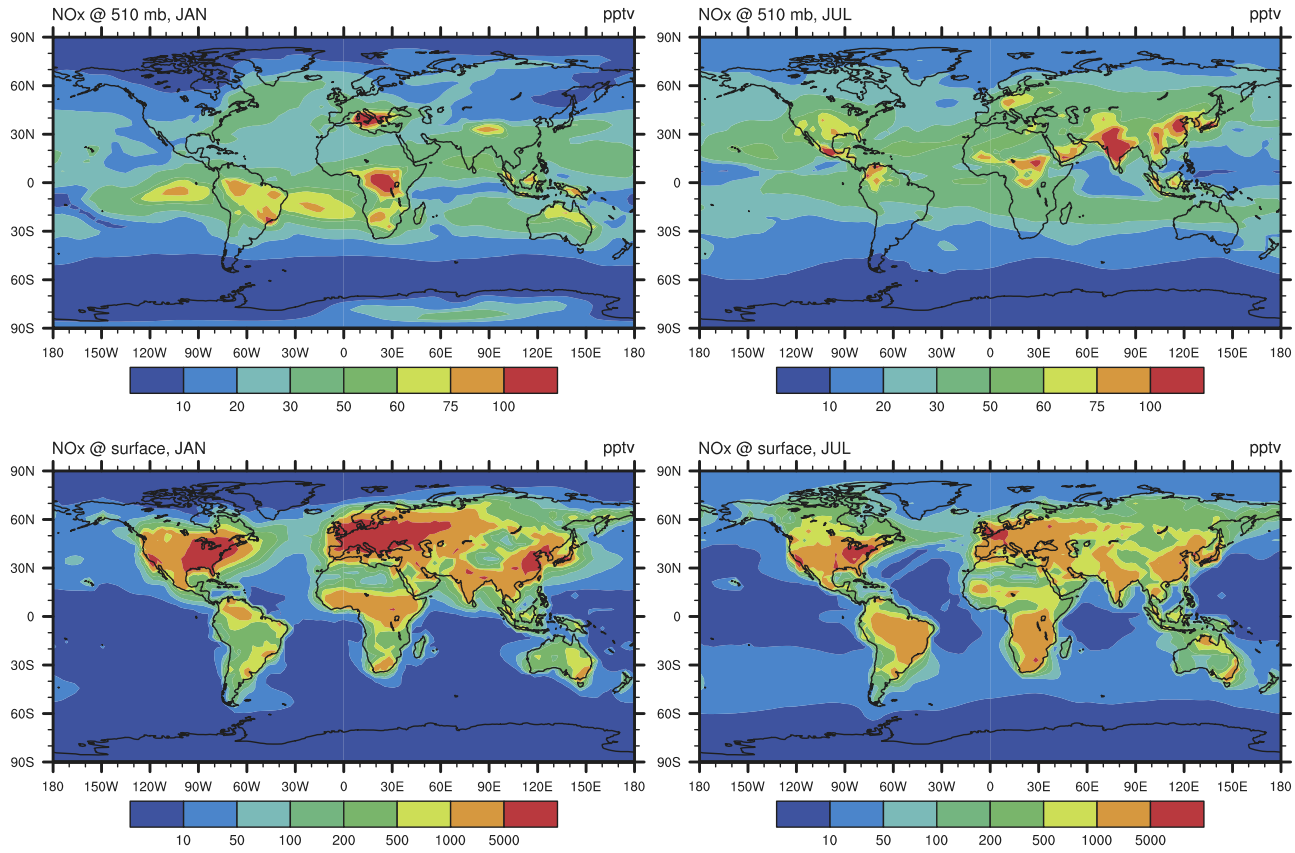

Figure 5. Same as Figure 2 but for NO_x (NO + NO_2) (in pptv).

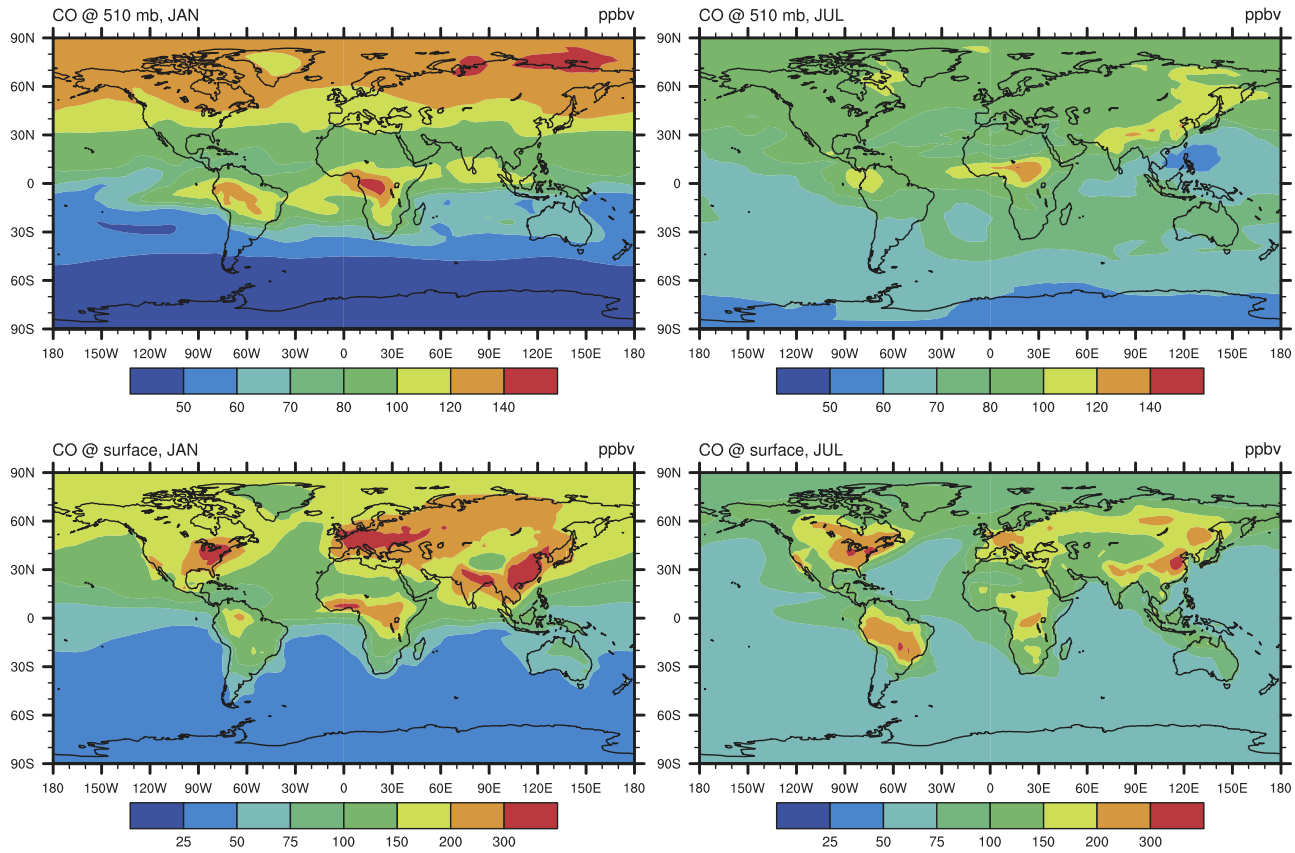

Figure 10. Same as Figure 2 but for CO (in ppbv).